CAPITAL UNIVERSITY OF SCIENCE AND TECHNOLOGY, ISLAMABAD

Planar MIMO Antennas for Sub-6 GHz and Millimeter-wave 5G Applications

by

Suleman Khan

A thesis submitted in partial fulfillment for the degree of Master of Science

in the

Faculty of Engineering
Department of Electrical Engineering

2022

Dedicated to my family

CERTIFICATE OF APPROVAL

Planar MIMO Antennas for Sub-6 GHz and Millimeter-wave 5G Applications

by

Suleman Khan

(MEE181019)

THESIS EXAMINING COMMITTEE

S. No.	Examiner	Name	Organization
(a)	External Examiner	Dr. Zubair Ahmed	NUST, Islamabad
(b)	Internal Examiner	Dr. M. Ashraf	CUST, Islamabad
(c)	Supervisor	Dr. M. Mansoor Ahmed	CUST, Islamabad

Dr. M. Mansoor Ahmed
Thesis Supervisor
May, 2022

Dr. Noor Muhammad Khan
Head
Dept. of Electrical Engineering
May, 2022

Dr. Imtiaz Ahmad Taj
Dean
Faculty of Engineering
May, 2022

Author's Declaration

I, **Suleman Khan** hereby state that my MS thesis titled "**Planar MIMO Antennas for Sub-6 GHz and Millimeter-wave 5G Applications**" is my own work and has not been submitted previously by me for taking any degree from Capital University of Science and Technology, Islamabad or anywhere else in the country/abroad.

At any time if my statement is found to be incorrect even after my graduation, the University has the right to withdraw my MS Degree.

(Suleman Khan)
Registration No: MEE181019

Plagiarism Undertaking

I solemnly declare that research work presented in this thesis titled "**Planar MIMO Antennas for Sub-6 GHz and Millimeter-wave 5G Applications**" is solely my research work with no significant contribution from any other person. Small contribution/help wherever taken has been duly acknowledged and that complete thesis has been written by me.

I understand the zero tolerance policy of the HEC and Capital University of Science and Technology towards plagiarism. Therefore, I as an author of the above titled thesis declare that no portion of my thesis has been plagiarized and any material used as reference is properly referred/cited.

I undertake that, if I am found guilty of any formal plagiarism in the above titled thesis, even after award of MS Degree, the University reserves the right to withdraw/revoke my MS degree and that HEC and the University have the right to publish my name on the HEC/University website on which names of students are placed who submitted plagiarized work.

(Suleman Khan)
Registration No: MEE181019

List of Publications

It is certified that following publication(s) has been made out of the research work that has been carried out for this thesis:-

1. U. Rafique, **S. Khan**, M. M. Ahmed, S. H. Kiani, S. M. Abbas, S. I. Saeed, M. Alibakhshikenari, and M. Dalarsson, "Uni-planar MIMO antenna for sub-6 GHz 5G mobile phone applications," *Applied Sciences*, vol. 12, no. 8, p. 3746, 2022.

(Suleman Khan)

Registration No: MEE181019

Acknowledgement

I humbly praise and grateful to **ALMIGHTY ALLAH**, Who permits me to live and accomplish tasks, including the research work presented in this thesis.

I would like to express my gratitude to my advisor **Prof. Dr. M. Mansoor Ahmed**, Vice Chancellor, Capital University of Science and Technology (CUST), Islamabad, for his support, encouragement, and mentorship. I would like to thank him because of the opportunity he has given me to follow and fulfill my research interests. I am so grateful for what I have learned from his gracious personality.

Thanks to **Mr. Umair Rafique**, PhD Researcher, Sapienza University of Rome, Rome, Italy, for his good ideas, support in research work, and in the fabrication and testing of antenna. I am thankful to the administration of CUST for providing me with an excellent environment perfect for conducting research. I am also thankful to Dean, Faculty of Engineering, **Prof. Dr. Imtiaz Ahmad Taj**, Head of Electrical Engineering Department, **Prof. Dr. Noor M. Khan**.

I also wish to express my feelings of gratitude to my father, mother, wife, brothers, and sisters, who prayed for my health and brilliant future. I would not have achieved these goals without their sincere co-operation and love. I am also using this opportunity to thank all my friends who prayed for me and encouraged me through their love and sincerity.

(Suleman Khan)

Abstract

The 5G system is expected to have a data rate 1000 times higher compared to 4G communication system. By incorporating multiple transmissions as well as the antennas and by decreasing multipath fading effects, the data rate can be increased in MIMO antennas. One of the keys to increasing the channel capacity of MIMO systems is to design multiple antennas for independent channels. In addition, the antennas should be small and low-profile that can easily fit into hand-held devices. Furthermore, a low mutual coupling MIMO antenna is required for 5G mobile communication system.

To fulfill the above mentioned requirements, in the first part of the thesis, a uni-planar MIMO antenna is designed for sub-6 GHz mobile phone applications. The proposed design consists of four loop-type radiation elements placed at the corners of the mainboard of the mobile phone exhibiting pattern diversity configuration. From the presented results, it is demonstrated that the antenna elements are resonating at 3.5 GHz. According to $S_{11} \leq$ -6 dB threshold, the impedance bandwidth of the MIMO antenna is 1.38 GHz (2.98–4.36 GHz), while for $S_{11} \leq$ -10 dB, it is 600 MHz (3.21–3.81 GHz) with isolation of >10 dB between the antenna elements. Furthermore, a gain of >3.5 dBi and radiation efficiency of >90% are achieved. The presented MIMO antenna provides sufficient radiation coverage supporting different sides of the mobile phone PCB, which is a useful characteristic for future 5G-enabled smartphones. In addition, the human hand and head effects on antenna performance are studied and acceptable properties are observed in the data and talk mode.

In the second part of this research work, additionally, a compact phased array is designed for mm-wave applications. Eight loop-type elements are arranged linearly so that they can easily be integrated on the smartphone board. The designed phased array is able to provide a wideband response as well as high gain with beam steering performance. From the presented results, it can be observed that the designed MIMO antenna is a good candidate for future 5G-enabled mobile phones.

Contents

List of Figures

List of Tables

Abbreviations

1G	First Generation
2G	Second Generation
3G	Third Generation
3-D	Three-dimensional
4G	Fourth Generation
5G	Fifth Generation
ARC	Active Reflection Coefficient
CDF	Cumulative Distribution Function
DG	Diversity Gain
ECC	Envelope Correlation Coefficient
FBR	Front-to-Back Ratio
FCC	Federal Communications Commission
GSM	Global System for Mobile Communication
IoT	Internet of Things
ITU	International Telecommunication Union
LTE	Long Term Evolution
MIMO	Multi-input Multi-output
mm-wave	Millimeter-wave
PCB	Printed Circuit Board
SAR	Specific Absorption Rate
SLL	Sidelobe level
SMS	Short Message Service
SNR	Signal-to-Noise Ratio
TARC	Total Active Reflection Coefficient

Wi-Fi	Wireless Fidelity
WiMAX	Worldwide Interoperability for Microwave Access
WLAN	Wireless Local Area Network

Symbols

Ω	Solid angle
λ_0	Free-space wavelength
λ_g	Guided wavelength
ε_r	Relative permittivity
ε_{reff}	Effective relative permittivity
ξ	Relative phase amplitude
c	Speed of light
d	Distance between antenna elements
f_r	Resonant frequency
$\vec{S_i}(\theta,\phi)$,$\vec{S_j}(\theta,\phi)$	Radiation characteristics of antenna i and j
S_{nn}, S_{mm}	Reflection coefficient
S_{nm}, S_{mn}	Transmission coefficient
Z	Impedance
Z_{ii}	Self-impedance
Z_{ij}	Mutual-impedance
η	Antenna efficiency

Chapter 1

Introduction

1.1 Introduction

After every 10 years, a new generation come after the deployment of first-generation (1G) mobile networks in 1982, and these generations are developed with time to fulfill the needs of mobile users. These trends will continue to grow because mobile traffic is exponentially increasing each year worldwide [1]. The mobile communication generations, which are developed till date are listed in Table 1.1. From the data of the table, it is observed that each communication generation has specific features, and they differ from each other in terms of data rate, and frequency bands.

When it comes to the mobile communication technologies, it refers to the overall speed, technology, frequency, and system. Each generation has its unique features. The 1G cellular communication network was introduced in the late 1970s and it was fully implemented in 1980s [2]. The 1G communication technology was based on analogue signals, which means that higher frequency was used for the modulation of voice signal. However, analogue signals degrade over time and space, resulting in call quality issues.

The second generation (2G) introduced the Global System for Mobile Communication (GSM) technology in the early 1990s. It allowed data and digital voice

TABLE 1.1: Brief overview of mobile communication generations [3].

Generations	1G	2G	3G	4G	5G
Deployment Year	1981	1992	2001	2010	2020
Data Rate	2 Kbps	64 Kbps	2 Mbps	100 Mbps	10 Gbps
Frequency Bands	900 MHz	900/1800 MHz	800/900 MHz 1700-1900 MHz 2100 MHz	800/900 MHz 1800 MHz 2100/2600 MHz	2.5/3.5/5.8 GHz 28/38 GHz 60 GHz

communication, and also improved security with the help of Signaling and Data Confidentially (SDC) and Mobile Station Authentication (MSA). As a result, many important services, such as Short Message Service (SMS), international roaming, conference calls, and call hold, were developed.

In 2001, the research community set goals for third generation (3G) mobile communications for improving voice and data capacity, increasing throughput and data transfer, and supporting a broader range of applications [4]. For the first time, 3G communication technology supports fixed wireless and high speed internet access, which accommodates video calling, online mobile gaming, mobile TV, navigational maps, and digital services. Compared to 2G, 3G technology offers enhanced security features, e.g. application and domain security, and secured network access.

In 2010, the fourth generation (4G) of mobile communication technology was released, with the goal of providing mobile consumers with increased speed, capacity, and quality, as well as improved security, lower-cost voice and data services, and internet over IP [5].

The 4G communication technology also introduced the Long Term Evolution (LTE) standard, which supports IP networking and packet switching. However, LTE was not able to fulfill all the specifications, but its advanced version did it [6]. The LTE-Advanced 4G networks utilized 40 different frequency bands [4, 6] and was able to provide 1 Gb/s peak data rate with the use of technologies such as Multi-input Multi-output (MIMO) and carrier aggregation [7].

1.2 Needs for 5G Technology

The current 4G is going to be replaced very soon with 5G to meet the requirements of high rate traffic consumption worldwide and open another advanced chapter of the telecommunication industry. 5G communication technology is measured beyond 2020 mobile communications technologies. Since the first standard generation introduced in 1982; in every 10 years, there have been new standards introduced to serve mobile users. But, with the rapid increase of mobile traffic, it is expected that the user's percentage will continue to increase in next decades, and the present 4G cellular system will be unmanageable in the long term. The major concern of 5G systems is to provide improved capacity with lower cost compared to the 4G systems, as capacity is directly proportional to the demands of users for higher and faster data rates.

According to several research organizations, Advanced 5G mobile technologies are expected to give a high data rate of 10 Gbps for stationary users, 1 Gbps for moving users, and greater than 100 Mbps in metropolitan regions [3].

Consumers will benefit from new features provided by 5G communication technology. It will give users an option to choose the best performing technology, such as Wireless Local Area Network (WLAN), Wireless Fidelity (Wi-Fi), 4G, and so on. The optimum performance will be determined not only by throughput, but also by the most appropriate metrics based on its applications.

1.3 5G Frequency Bands

The mobile communication industry facing challenges about particular choices and at this stage, the entire frequency range up to 100 GHz is under consideration for 5G services. Recently, various organizations carried out considerable research on a global scale on the feasibility of spectrum below 6 GHz for wide-area coverage and outdoor to indoor communication. Lower frequency bands are preferred from the point of view of propagation properties. So, the possible frequency bands for 5G

communication could be 470–694 MHz, 1.427–1.518 GHz, 3.3–3.7 GHz, 4.8–4.99 GHz. Specific candidate spectrum above 6 GHz is yet needed to be identified by the International Telecommunication Union (ITU) or individual regulatory bodies [8].

In order to ensure a high data rate in 5G technology, a huge bandwidth is required, which can be achieved by using higher frequency bands [9]. Millimeter-wave (mm-wave) frequency bands are the greatest solution for achieving high bandwidth and high data rate. ITU allocated some frequency bands for mm-wave communication, which are 24.25–27.5 GHz, 37–40.5 GHz, 42.5–43.5 GHz and 60 GHz [10]. It is worth mentioning that frequencies above 10 GHz will be used as an additional spectrum with lower frequency bands to accommodate 5G services [11]. This kind of integration will provide high data rate, wide bandwidth, and enhanced system capacity in dense deployments [8, 12].

1.4 Need of Antennas for 5G Technology

The design of the air interface is generally dependent on the design of the antenna. Owing to the strict requirements of 5G technology, it requires a complete re-designing of the devices. Therefore, this requires the design and validation of next-generation antennas that exhibit features, which are not present in the previous generations. Moreover, the antennas need to accommodate the needs set by the upcoming transceiver technologies in 5G like the Massive MIMO, reduced RF MIMO, etc. Also, due to the small dimensions of hand-held devices, compact, low-cost, and low loss printed antennas are required that can easily be integrated with 5G circuitry [13, 14].

Planar antennas have gotten a lot of interest in recent years for a variety of microwave and mm-wave applications due to their small size, low fabrication cost, and ease of integration for portable devices. Furthermore, antennas can be built smaller in size but at the same time without compromising its operating efficiency [15]. On the other hand, the small antenna size can enable sharp beamforming

and can also lead to massive MIMO technology to achieve increased network capacity and throughput. The detailed discussion on the MIMO antenna system is provided in the next section.

1.5 MIMO Antenna System

Advanced cellular and wireless communication technologies such as LTE introduced MIMO technology to achieve high data rate without utilizing additional spectrum [16]. MIMO technology creates multiple uncorrelated channels in a scattering environment by using multiple antennas, which can result in higher throughput and data rates, as well as a higher received Signal-to-Noise Ratio (SNR) and greater interference robustness [17].

The concept of MIMO was first investigated in 1990s where the aim is to increase wireless system capacity [18, 19]. Figure 1.1 illustrates a generic representation of a MIMO system. In a MIMO communication system, M transmitting and N receiving antennas are employed. All transmitting antennas may send signals to each receiving antenna, resulting in transmission lines of $M \times N$. These transmission paths will be utilized to transmit multiple independent data streams. Furthermore, provided that, both the transmitter and receiver sides have negligible signal and noise correlation, the MIMO system capacity will rise linearly with the number of transceiver antennas $\min(M, N)$ [18, 19]. Due to this advantage, MIMO technology has become an integral component of numerous wireless communication standards, including Worldwide Interoperability for Microwave Access (WiMAX), 4G LTE, and 5G.

1.5.1 Diversity Techniques for MIMO

Frequency diversity, time diversity, and antenna diversity are commonly employed to reduce spatial correlation between antenna elements and generate duplicates of a signal for diversity purpose. For particular application, antenna diversity

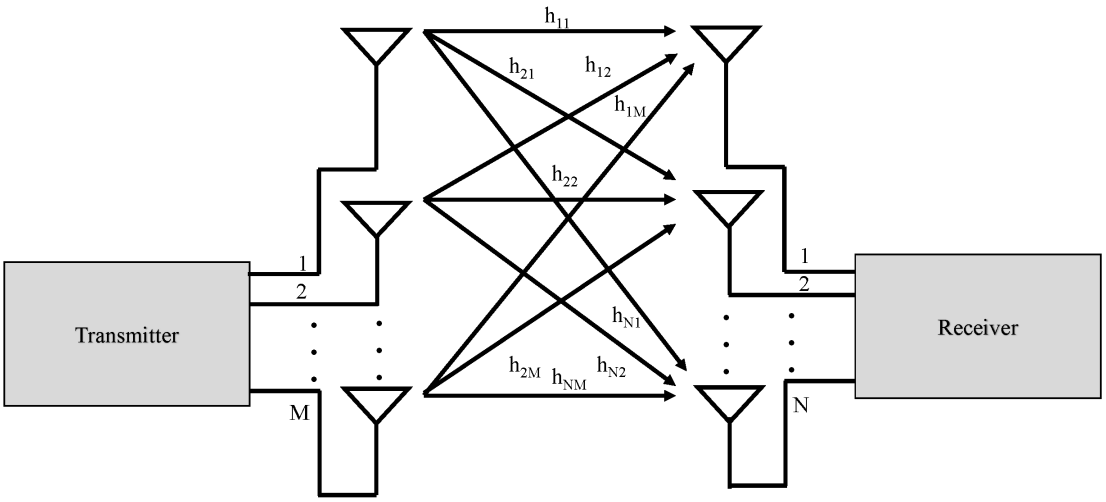

FIGURE 1.1: Generic representation of a MIMO system.

is discussed in detail, which consists of spatial diversity, pattern diversity, and polarization diversity.

1.5.1.1 Spatial Diversity

One of the simplest and most commonly used antenna diversity in wireless communication systems is the spatial or free-space diversity [20, 21] as shown in Fig. 1.2(a). In this technique, antennas are placed at two points in space.

Due to the phase difference, the fading signal in the second antenna may be uncorrelated with the first. Depending on the surrounding environment, the spacing between the antennas must be reduced to provide proper decorrelation [20, 21].

1.5.1.2 Pattern Diversity

The Diversity Gain (DG), which is the fundamental parameter to access MIMO antenna performance will be maximum if antennas have different radiation patterns. The MIMO antenna system with pattern diversity comprises of more than one antennas with various radiation patterns as shown in Fig. 1.2(b).

When compared to a single antenna with an omnidirectional pattern, these MIMO antennas can discriminate a large amount of angle space and deliver a high gain

[22]. Pattern diversity can also ensure the reception of many sets of multipath waves, which is beneficial for achieving high channel capacity and data throughput [22, 23].

1.5.1.3 Polarization Diversity

Polarization diversity, as opposed to spatial diversity, allows antennas to be placed in the same location but with distinct polarizations as shown in Fig. 1.2(c). It has been demonstrated that using a dual-polarized antenna system can produce channel capacity similar to that obtained through spatial diversity [24].

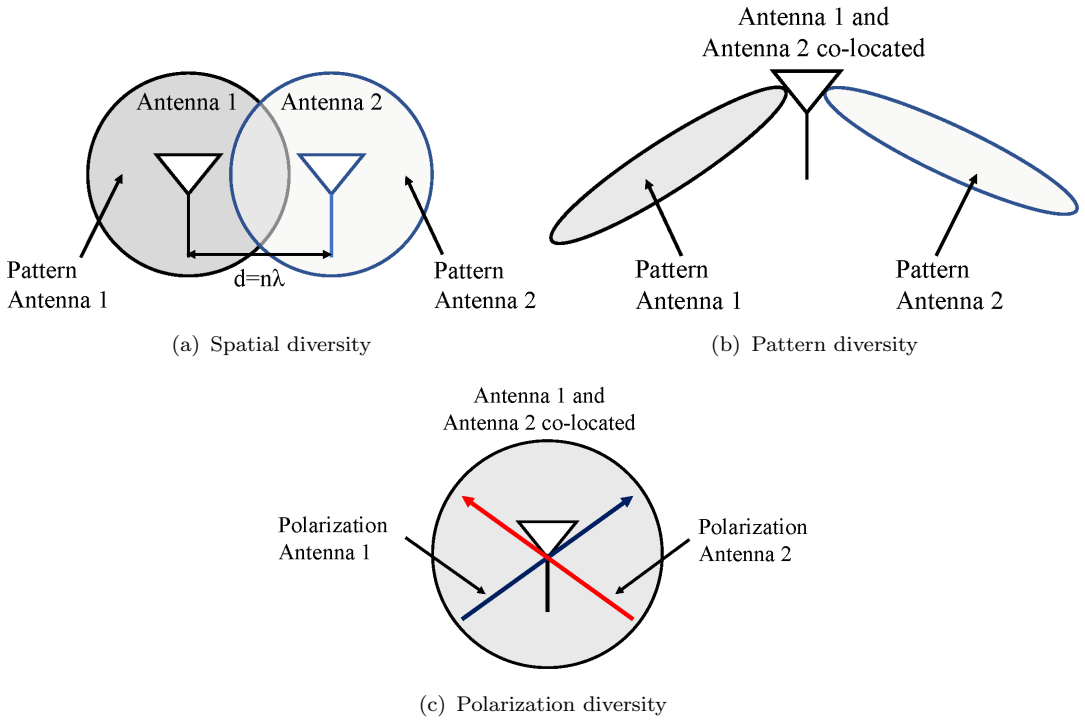

(a) Spatial diversity

(b) Pattern diversity

(c) Polarization diversity

FIGURE 1.2: Antenna diversity techniques.

1.5.2 MIMO Key Parameters

Since the introduction of MIMO technology, researchers have devoted special attention to the design of numerous antenna elements at both transmitter and reciever sides. This demand also arises some challenges such as the implementation of multiple antennas on lesser area on a Printed Circuit Board (PCB). Unlike

single antenna system, MIMO antenna technology requires more performance parameters that need to be analyzed. These new performance parameters are named as mutual coupling, Envelope Correlation Coefficient (ECC), and DG [25]. The performance parameters of single antenna such as bandwidth, radiation efficiency, gain are also required to characterize MIMO antennas [26].

1.5.2.1 Mutual Coupling

Mutual coupling is the interaction between antenna elements caused by the integration of several antennas in a small space [58]. Mutual coupling is caused by induced current flowing through one antenna as a result of the other antenna's excitation.

As a result of this impact, the input impedance (Z_{in}) of each antenna element will be changed, which is defined by both mutual (Z_{ij}) and self-impedance (Z_{ii}) which can be expressed as:

$$Z = \begin{bmatrix} Z_{11} & \cdots & Z_{1N} \\ \vdots & \ddots & \vdots \\ Z_{N1} & \cdots & Z_{NN} \end{bmatrix} \tag{1.1}$$

As a result of above-mentioned matrix, antenna bandwidth can be determined by evaluating both the reflection and transmission coefficients, which can be stated using the S-parameters matrix as:

$$S = \begin{bmatrix} S_{nn} & \cdots & S_{nm} \\ \vdots & \ddots & \vdots \\ S_{mn} & \cdots & S_{mm} \end{bmatrix} \tag{1.2}$$

In the above matrix, S_{nn} and S_{mm} corresponds to the the ratio of the reflected wave to the incident wave, while S_{nm} and S_{mn} represents the ratio of the transmitted wave to the incident wave. S_{nm} and S_{mn} also represent the mutual coupling between antenna elements [26].

1.5.2.2 Envelope Correlation Coefficient (ECC)

The received signals at the receiver side should be independent of each other in order to produce strong diversity performance, which may be determined by examining the ECC [25, 27–29]. Generally, ECC can be calculated using far-field radiation characteristics as [30]:

$$\mathrm{ECC} = \frac{|\iint_{4\pi}(\vec{M}_i(\theta,\phi)) \times (\vec{M}_j(\theta,\phi))d\Omega|^2}{\iint_{4\pi}|(\vec{M}_i(\theta,\phi))|^2 d\Omega \iint_{4\pi}|(\vec{M}_j(\theta,\phi))|^2 d\Omega} \tag{1.3}$$

where $\vec{M}_i(\theta,\phi)$ and $\vec{M}_j(\theta,\phi)$ describe the radiation characteristics of antennas i and j, respectively; and Ω denotes the solid angle.

As the S-parameters based definition of ECC is used for high efficiency antennas as well as these calculations using 3-D radiation characteristics are time-consuming, therefore, Hallbjorner has proposed a simplified approach to approximate the ECC for a two port network when only S-parameters and efficiencies are known [29]:

$$\mathrm{ECC} = \frac{|S_{11}S_{12}^* + S_{21}S_{22}^*|^2}{\left(1-|S_{11}|^2-|S_{21}|^2\right)\left(1-|S_{22}|^2-|S_{12}|^2\right)\eta_1\eta_2} \tag{1.4}$$

where η_1 and η_2 corresponds to MIMO antenna's efficieny. For good diversity performance, the value of ECC should be $\leq$0.5 [27, 28].

1.5.2.3 Diversity Gain (DG)

The MIMO system's DG refers to the increase in received SNR at the diversity combiner's output [25]. It can easily be evaluated using the calculated and measured Cumulative Distribution Function (CDF), during this process, some of the information might be lost such as the frequency range of the system. Because in MIMO systems, it is of great importance to know how DG varies with respect to frequency. For this purpose, the ECC of the system can be used for the calculation of DG as [31, 32]:

$$\mathrm{DG(dB)} = 10\left(\sqrt{1-\mathrm{ECC}^2}\right) \tag{1.5}$$

1.5.2.4 Total Active Reflection Coefficient (TARC)

Total active reflection coefficient (TARC) is defined as "the ratio of reflected power to the incident power". In MIMO antenna systems, TARC is mostly used instead of scattering parameters to characterize the radiation efficiency and band-width of the antenna array. For N-elements, TARC can be estimated as [33]:

$$\text{TARC} = \sqrt{\frac{\sum_{i=1}^{N} |b_i|^2}{\sum_{i=1}^{N} |a_i|^2}} \tag{1.6}$$

where a_i and b_i are the incident and reflected signals, respectively. For multi-port network having same characteristic impedances (Z_0), the relationship between a_i and b_i is given by [34]:

$$\boldsymbol{b} = \boldsymbol{S}\boldsymbol{a} \tag{1.7}$$

where **S** relates to the S-parameters matrix. For example, for an N-port network, the **S** matrix can be written as $N \times N$. TARC for a 2-port network can be written as:

$$\text{TARC} = \sqrt{\frac{|S_{11} + S_{12}e^{j\theta}|^2 + |S_{21} + S_{22}e^{j\theta}|^2}{2}} \tag{1.8}$$

1.6 Research Motivation

With the sudden advancement of cellular communication systems, cellular communication networks have evolved into a heterogeneous network environment capable of supporting several frequency bands for various cellular generations. The 1G was released in order to allow analogue voice calls. The 2G was later upgraded to include new features such as SMS and digital voice calls. After that, 3G technology includes multimedia services as well as high-speed internet, high-definition video, and voice calls. Finally, 4G was introduced whose main purpose is to provide high-speed internet services over harsh multipath channels.

5G cellular networks are considered to be a viable alternative for overcoming current communication technology limitations. The mm-wave spectrum (24 GHz, 28

GHz, 37–39 GHz, and 60 GHz) has been recommended by the Federal Communications Commission (FCC) as the operational frequency for 5G communication. However, the proposed spectrum has issues and flaws in terms of propagation, which could have an impact on network implementation. As a result, the 5G mid-band (3.3–3.7 GHz) has been designated by the ITU for broadband cellular communication systems.

The sub-6 GHz band, commonly known as the 5G mid-band, can provide more coverage over a bigger area while minimizing propagation losses. The 5G mm-wave frequency bands are ideal for dense 5G small-cell networks in metropolitan regions with increased capacity demands, as well as macro-cells that give more coverage. To accommodate a considerable volume of traffic at a high data rate, 5G services require roughly 100 MHz bandwidth in the sub-6 GHz spectrum and 1 GHz bandwidth in the mm-wave band. In addition, a MIMO antenna system for 5G communication systems is required to fulfill the high data rate and increased channel capacity needs.

In this thesis, a 4×4 MIMO antenna system is designed for sub-6 GHz (3.5 GHz) 5G-enabled smartphone applications, taking into account the aforementioned need. Four loop-shaped radiators are placed at each corner of a smartphone board to form a uni-planar pattern diversity based MIMO antenna system. Different diversity performance parameters, such as ECC, DG, and Total Active Reflection Coefficient (TARC) are discussed in detail. Furthermore, to accommodate mm-wave band, a compact phased array is designed for 28 GHz frequency band. The designed phased array provides wide bandwidth and beam steering performance for scanning angles up to 90°.

1.7 Thesis Organization

This chapter presents details pertaining to cellular communication systems and MIMO technology. The chapter starts with the introduction of previously deployed communication networks, such as 1G, 2G, 3G, and 4G. A detailed discussion is

also provided on 5G communication system that why 5G networks are considered to be a good candidate for future technologies. Different frequency bands used in 5G communication systems are discussed in detail. After that, a discussion is provided on MIMO antenna system, different diversity techniques, and MIMO performance parameters. The remaining organization of the thesis is given below:

Chapter 2 presents a detailed overview of previously presented MIMO antenna designs for sub-6 GHz and mm-wave 5G communication applications. The chapter starts with the discussion of non-planar and planar MIMO antenna arrays presented in the literature along with their performance. Different phased arrays techniques and configuration meant for mm-wave applications are also discussed in detail.

Chapter 3 describes a 4-element sub-6 GHz MIMO antenna design 5G applications. The designed array is uni-planar in nature and followed the principle of pattern diversity technique. The simulation as well as measured results show that the designed array has wide impedance bandwidth and acceptable radiation characteristics. The performance of the designed MIMO array is also accessed in the presence of user.

Chapter 4 presents a phased array design for 28 GHz applications that can easily be integrated with the sub-6 GHz MIMO antenna. The designed phased array provides wide impedance bandwidth, high gain, beam steering performance for different scanning angles that is useful for mm-wave communication systems.

Chapter 5 discusses the conclusion drawn from this research and its extension as future work.

Chapter 2

Literature Survey

The designs and configurations of previously described MIMO antenna arrays for sub-6 GHz 5G mobile phone applications are presented in this chapter. The design techniques of the MIMO antennas are discussed in detail along with their performance parameters. In addition, the phased arrays designed for mm-wave applications are also discussed in this chapter.

2.1 Sub-6 GHz MIMO Antennas

Many researchers have designed different MIMO array configurations for sub-6 GHz mobile phone applications. These arrays are either non-planar and planar.

In [35], a 10-element MIMO configuration was developed for mobile services.. The single antenna component of the MIMO arrangement was comprised of a T-formed resonator supplied by an L-formed microstrip line as shown in Fig. 2.1(a). Two components were positioned on the upper and lower sides of the printed circuit board (PCB), and the rest of the six elements were located on the other sides of the PCB, respectively. The MIMO array was shown to have resonance in two frequency ranges, 3.5 GHz and 5.5 GHz. More than 10 dB of isolation between the antenna components was found to exist for 3.5 GHz frequency range and more than 15 dB isolation was found to exist for the 5.5 GHz frequency band, respectively.

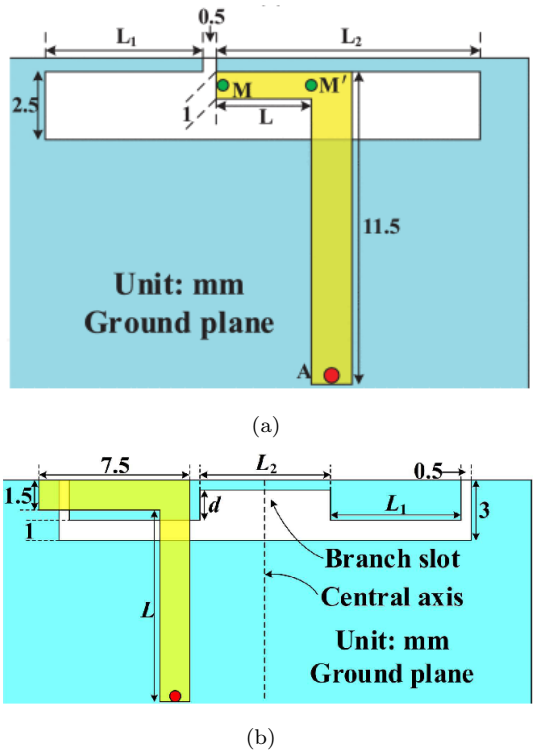

FIGURE 2.1: Schematic of the (a) T-shaped slot antenna [35] and (b) balanced open branch slot antenna [36].

Furthermore, the designed MIMO system demonstrated overall efficiency of >42% and >62% for both bands, respectively.

In [36], an eight-component MIMO structure was developed for 3.5 GHz spectrum. A symmetrical open fork slit antenna with an L-shaped feeding strip was designed as shown in Fig. 2.1(b). This configuration offers isolation of >17.5 dB between antenna elements, but the design suffers because of poor antenna efficiency. Moreover, the performance of the designed array was accessed and acceptable MIMO antenna characteristics was observed for both data mode and talk mode. Same kind of configuration with rectangular shaped slot was presented in Ref. [37]. The MIMO arrays consisted of two kind of antenna elements for different frequency operations. Two elements of same configuration were placed on the top and bottom corners of the PCB for 2G/3G/4G communication, while 6-elements meant to operate at 3.5 GHz were placed on left and right side of the PCB.

In [38], a compact 4×4 and 8×8 orthogonal mode MIMO antenna array was designed for mobile phone applications. Each antenna element consisted of a pair of

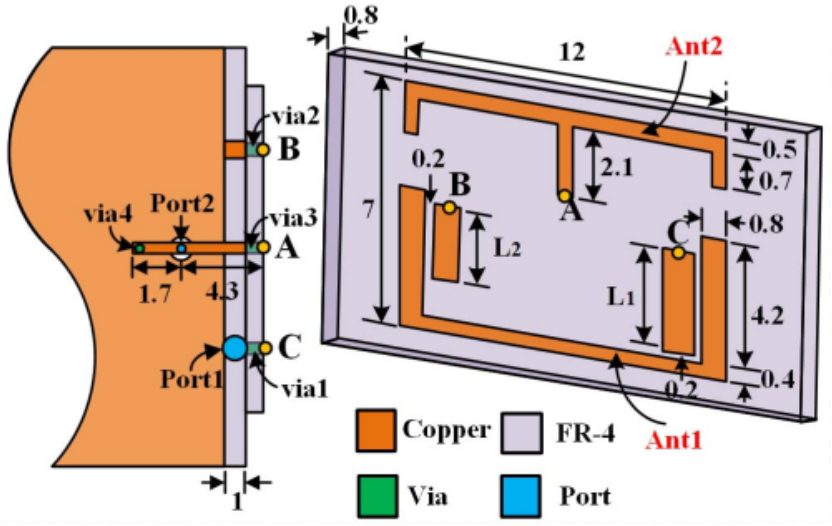

FIGURE 2.2: Configuration of the orthogonal mode antenna element designed for 5G sub-6 GHz applications [38].

bended monopole and an edge fed dipole as shown in Fig. 2.2. The orthogonal mode configuration was presented to achieve high isolation without utilizing an extra decoupling network.

Therefore, an isolation of >17 dB and >20 dB was achieved in the band of interest for 4×4 and 8×8 MIMO arrays. Moreover, the efficiencies of the designed arrays varied in the range of 51.7%–84.5% and 49%–72.9%, respectively. Same kind of configuration was presented in [39, 40]. In these designs, a common grounding branch was designed between the antenna elements, which behaves as a decoupler.

The authors in [41] designed eight-port broadband MIMO antenna for sub-6 GHz services. The design consisted of a single MIMO antenna of a 50Ω supply line with an open circuit tuning stub, a slot on the metal frame, and a U-shaped slot on the ground plane as shown in Fig. 2.3. The antenna provided a broadband response in the frequency range of 3.3-6 GHz, according to -6 dB impedance bandwidth requirements. The MIMO arrangement was achieved by adding eight antenna elements on the smartphone PCB's left and right sides.

In [30], a monopole slotted MIMO antenna was presented for 2.6/3.5 GHz bands. The four metal frame-based antennas fed using an L-shaped feed line were positioned in the middle of the PCB, with the other four elements on the top and

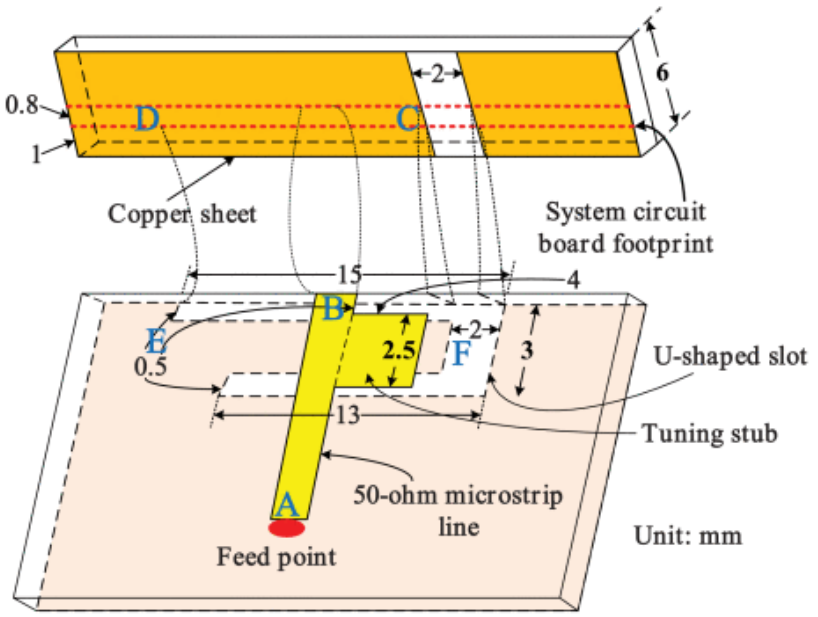

FIGURE 2.3: Schematic representation of metal frame based slot antenna [41].

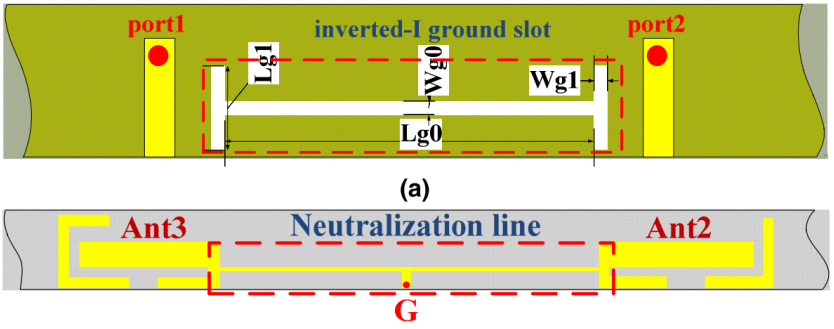

FIGURE 2.4: Geometry of the U-shaped loop, L-shaped loop, and decoupling structure [42].

bottom sides of the PCB. The planned MIMO structure offers satisfactory reflection and isolation performance in the operating bands.

In [42], a MIMO antenna array was designed for 3.5 GHz 5G smartphone applications. The array was made up of two distinct ways: one was an L-formed coupled-fed array and the other was a U-formed loop array, both of which were mounted on the smartphone's metal frame as shown in shown in Fig. 2.4. For isolation enhancement, the authors created an inverted-I slot and a neutralization line between the antenna components, resulting in 15 dB of isolation in the operational bandwidth.

In [43], a dual-polarized diamond ring slots, shown in Fig. 2.5(a), based MIMO

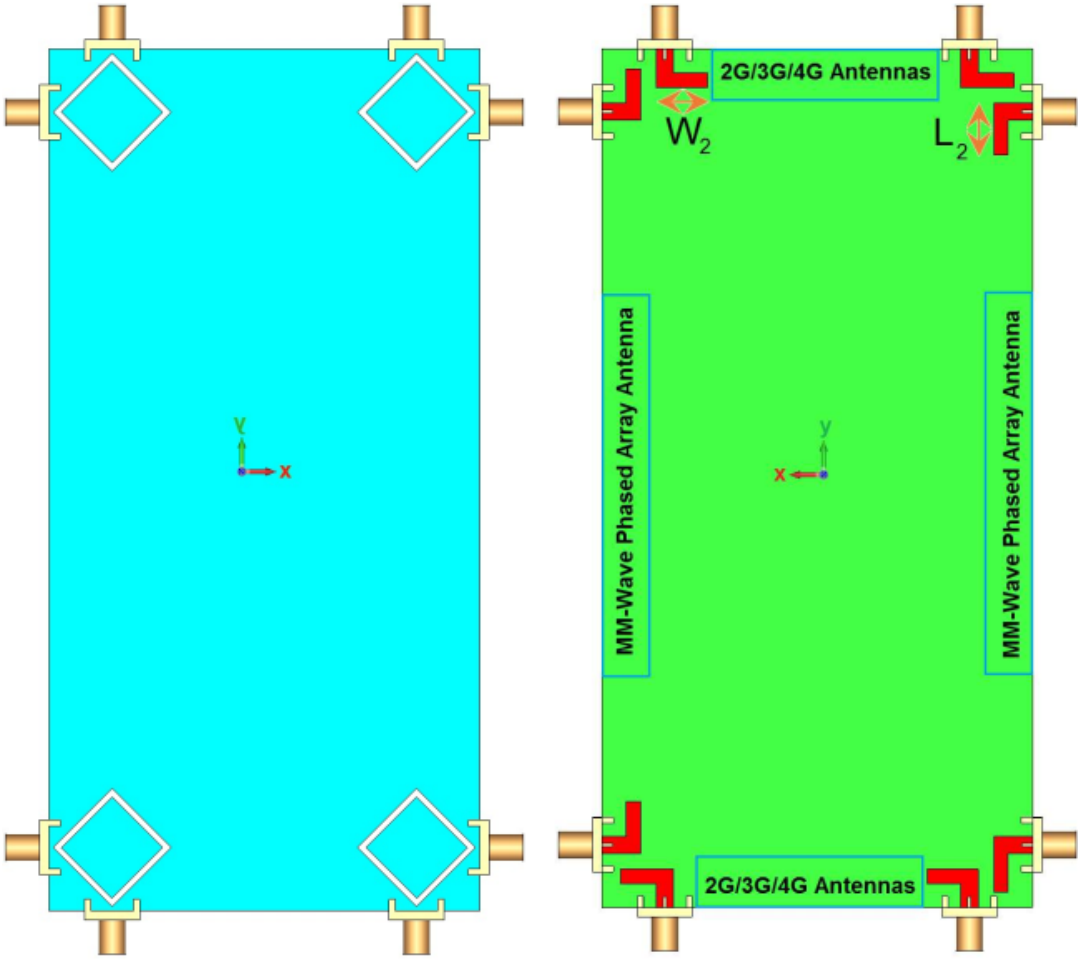

FIGURE 2.5: Schematic of the dual-polarized slot antenna designed on a mobile phone (a) back side and (b) front-side [43].

antenna was designed for 5G massive MIMO applications. Four dual-fed slot elements were placed on each corner of the mobile phone PCB. To feed the slot element an L-shaped microstrip feed line was used as shown in Fig. 2.5(b). The presented antenna configuration offered both polarization and pattern diversity due to the orthogonal placement of feed lines.

Moreover, the designed antenna element offered a stable gain of 3 dBi for the band of interest and >80% radiation and total efficiencies. In addition, an isolation of more than 20 dB was observed within the operating range.

In [44], same kind of configuration was utilized to design MIMO antenna array for sub-6 GHz applications. In the presented configuration, a circular-ring resonator

was etched from the ground plane and fed using orthogonally placed microstrip feed lines. The authors also designed a multi-band MIMO antenna by replacing the conventional microstrip feed line with a fork-shaped feed line. With the use of fork-shaped feed line, a multiple resonances was achieved at 3.6 GHz, 5.5 GHz, and 6.6 GHz.

In [45], a self-isolated 8-element MIMO antenna system was designed for 3.5 GHz frequency band. The dimensions of the antenna element was reduced by designing two vertical stubs into the antenna as shown in Fig. 2.6(a). It was demonstrated that this kind of configuration offered an isolation of ≥20 dB. Moreover, a T-shaped and inverted U-shaped radiating structures connected to the ground plane were utilized to achieve resonance for 3.5 GHz frequency band as depicted in Fig. 2.6(a). In addition, the designed MIMO system had a radiation efficiency of >65%. Same kind of configuration was presented in [46] but with meandered radiating strucutre as shown in Fig. 2.6(b). They also presented another self-isolated MIMO antenna in Ref. [47]. In this configuration, a T-shaped and two inverted L-shaped radiating structures were used. The MIMO antenna designs presented in [45–47] were designed on the metal frame of the smartphone. Wang et al. [48] also designed same kind of MIMO configuration for 5G mobile phone antennas.

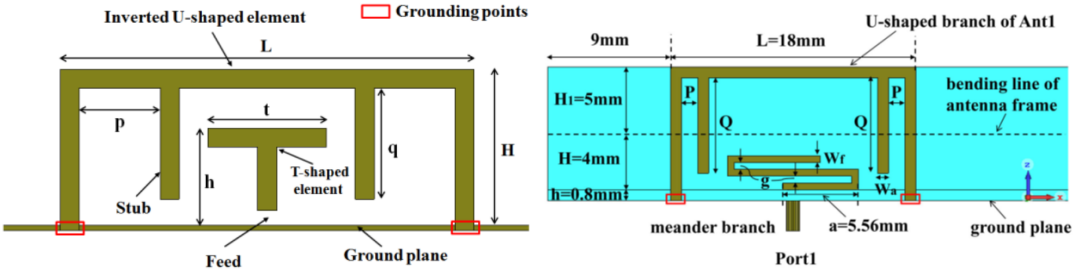

FIGURE 2.6: Configuration of the self-isolated antenna element with (a) T-shaped and inverted U-shaped radiator [45] and (b) meandered radiating structure [46].

In [49], an 8-port MIMO antenna based on an I-shaped element was developed for IoT and 5G technologies. To provide space for additional components, the cell-phone's metal frame was constructed to accommodate the antenna components. The antenna was found to resonate effectively in 3.5 GHz frequency band. The

MIMO antenna offers 13 dB of isolation between array elements, with a gain of 4 dBi and an antenna efficiency of more than 40%. In [50], an integrated MIMO antenna system for LTE and mm-wave frequency bands was designed. The designed antenna structure was comprised of two elements for LTE communications and 4-elements for 5G mm-wave communication as shown in Fig. 2.7(a). A modified rectangular radiator was utilized for both the frequency bands. Moreover, the antenna elements meant for mm-wave frequency band consisted of a 1×2 antenna array as shown in Fig. 2.7(a). In addition, defects in the ground plane were introduced using rectangular and circular shapes as illustrated in Fig. 2.7(b). The antenna element designed for LTE band provide resonance for 5.5 GHz frequency band, while the other was resonating for 28 GHz frequency band. Furthermore, an isolation of about 22 dB was observed for both the frequency bands.

A sub-6 GHz cellular MIMO loop antenna array was developed in [51]. The antenna components and ground plane were both placed on the same face of the PCB. The band of interest was served by a loop of eight antenna components organized in such a way as to offer polarization and pattern diversity as depicted in Fig. 2.8. Enhanced bandwidth (3.2–4 GHz) and isolation (>15 dB) were improved by applying a reconfigured arrow-formed strip between the antenna components.

A comparable MIMO setup was shown in [52]. A multi-mode PIFA (Planar Inverted-F Antenna) was employed instead of a loop-type component, and resonance was obtained in three distinct frequency bands of 2.5–2.7 GHz, 3.43–3.75 GHz, and 5.6–6 GHz, spanning all the major ones given to the sub-6 GHz spectrum.

In [53, 54], the authors designed a Co-planar Waveguide (CPW)-fed MIMO antenna arrays by following the design configurations presented in [43, 44, 51, 52]. An L-shaped and T-shaped radiation elements were selected for the design purpose. By utilizing CPW technique, an isolation of >15 dB was achieved in the band of interest. One of the MIMO antenna configuration is shown in Fig. 2.9.

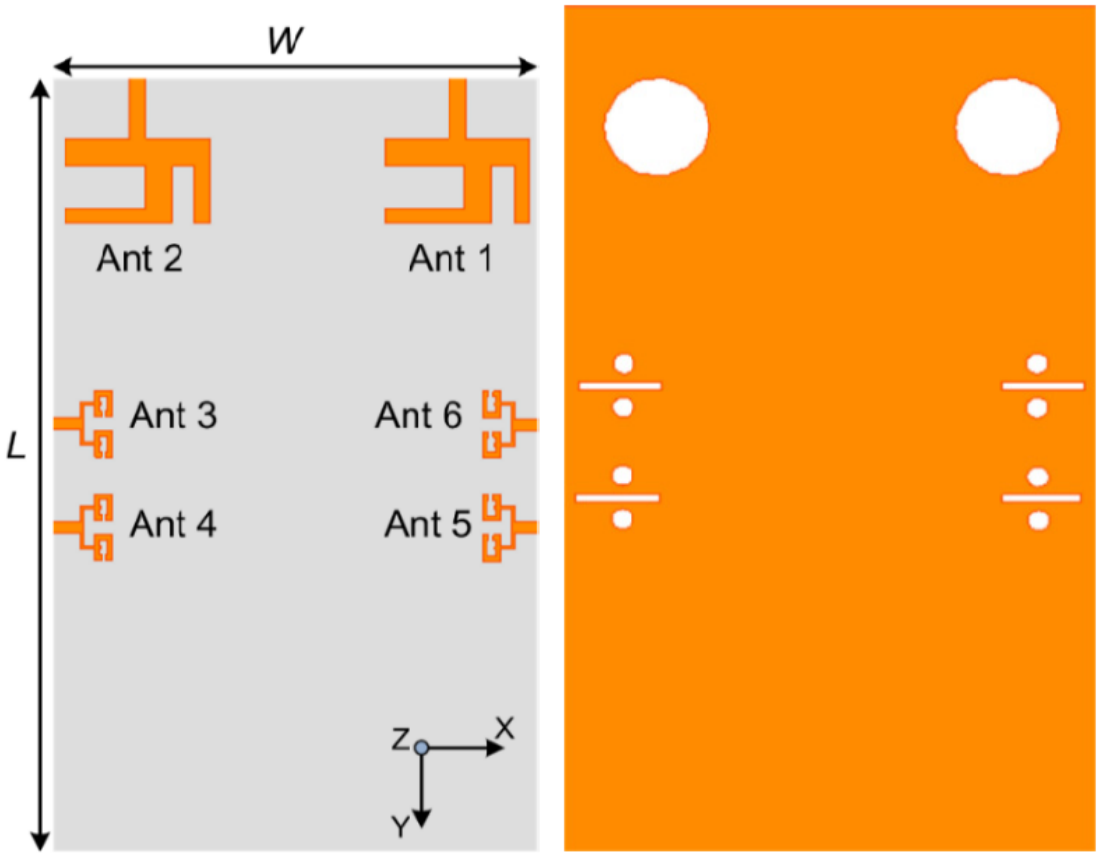

(a) (b)

FIGURE 2.7: Design of the integrated MIMO antenna system for LTE and mm-wave applications (a) top side and (b) bottom side [50].

Table 2.1 provides a brief summary of previously presented MIMO antenna arrays for sub-6 GHz applications.

TABLE 2.1: Brief summary of previously presented MIMO antenna arrays for sub-6 GHz mobile phone applications.

Author	**Year**	**Development**	**Ref.**
Li et al.	2018	Design of a T-shaped slot fed 10-elements based dual-band MIMO antenna array for 5G smartphones.	[35]
Sun et al.	2018	Design of bended monopole and edge fed dipole based orthogonal mode 4×4 and 8×8 MIMO arrays.	[38]

Zhao and Ren	2018, 2019	Self-isolated 8-element sub-6 GHz MIMO antenna cellular applications.	[45–47]
Zhang et al.	2019	Design and development of eight port MIMO antenna array with open circuit tuning stub, U-slot, and an open slot etched from the metal frame.	[41]
Abdullah et al.	2019	Eight element slotted monopole MIMO antenna design for 2.6 and 3.5 GHz frequency bands.	[30]
Jiang et al.	2019	Design of U-shaped loop and L-shaped coupled-fed MIMO antenna for 3.5 GHz applications.	[42]
Parchin et al.	2019	Dual-polarized diamond-ring based MIMO slot antenna for sub-6 GHz applications.	[43]
Li et al.	2019	A balanced open branch slot based 8-element MIMO antenna array design for 3.5 GHz.	[36]
Ullah et al.	2020	Design of a integrated 2G/3G/4G and sub-6 GHz antenna.	[37]
Parchin et al.	2020	Development of orthogonally dual-polarized pattern diversity-based MIMO antenna system for 5G smartphones.	[44]
Kiani et al.	2020	Design of an I-shaped element based 8-port MIMO antenna array.	[49]
Naqvi et al.	2020	Design of integrated LTE and mm-wave MIMO antenna system.	[50]
Parchin et al.	2020	Design of a broadband MIMO loop antenna array for sub-6 GHz cellular applications.	[51]
Parchin et al.	2020	Design of a multi-mode PIFA for sub-6 GHz 5G MIMO communication.	[52]

Parchin et al.	2020	Design of CPW-fed MIMO antenna arrays for sub-6 GHz applications.	[53, 54]

2.2 Millimeter-wave Phased Arrays

It is expected that the 5G-enabled devices should accommodate mm-wave frequency ranges in addition to the sub-6 GHz spectrum [55]. For this purpose, small size antenna arrays can be utilized at different portions of a smartphone PCB. In addition, phased arrays with high beam steering performance are desirable for mm-wave communication because they can increase the efficiency of the system. Therefore, to fulfill this requirement, many researchers designed different phased array configurations for mm-wave mobile phone applications.

In [56], a mesh-grid patch array was designed for mm-wave 5G-enabled smartphones. Two mesh-grid arrays having 16-elements were integrated on the top and bottom sides of the smartphones, and feed line of same electrical lengths were used to feed each antenna element of the arrays as shown in Fig. 2.10(a). The patch elements are made up of seven layers of stacked conducting vias, shown in Fig. 2.10(b), placed along the z-axis. The antenna's resonant frequency was tuned by optimizing the length of the mesh grid along the x-axis. On the 5^{th} layer of the PCB, the microstrip feed line was designed, which directly feed antenna elements through a via.

The characteristics of the antenna, such as reflection coefficient, gain, etc., was adjusted by optimizing the dimensions of the feed line. Furthermore, the phased array was created by using an RF beamforming scheme by controlling 16 6-bit external phase shifters. Therefore, the array was able to provide beam steering performance upto 75° scanning angle. But with the increase in scanning angle,

FIGURE 2.8: Representation of MIMO loop antenna array [51].

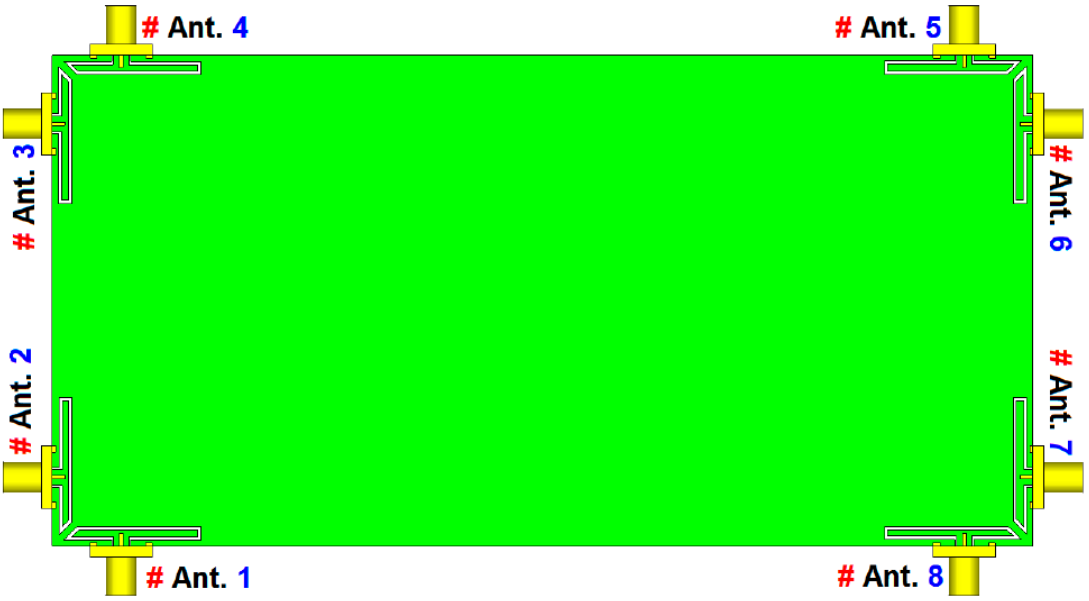

FIGURE 2.9: Design configuration of the CPW-fed T-shaped MIMO antenna [53].

the gain of the array was reduced upto 3 dB, which could be the effect of phase shifters.

In [57], the authors designed an air-filled slot-loop antenna array 5G mobile phone applications. The array consisted of 10 slot-loop type antenna elements placed along the edge of the smartphone PCB as shown in Fig. 2.11. According to the authors, the presented array can achieve high gain because air ($\varepsilon_r = 1$ and $\tan\delta$

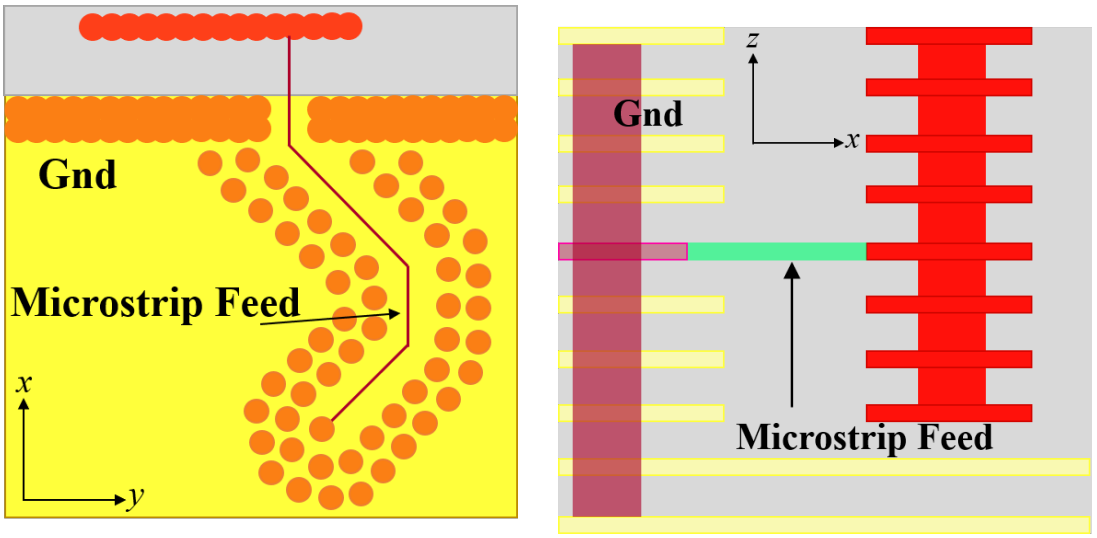

(a) (b)

FIGURE 2.10: Design topology of the mesh-grid patch antenna (a) top view and (b) side view [56].

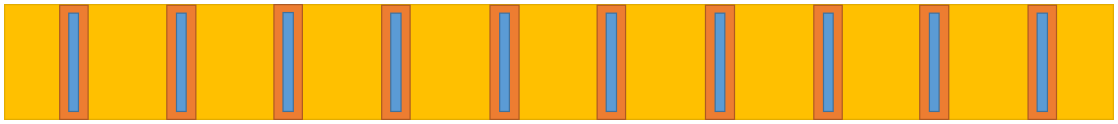

FIGURE 2.11: Geometry of the slot-loop antenna array for 28 GHz mobile phone applications [57].

= 0) was used as the main substrate for the design slot-loop elemets. The simulation results showed that the phased array was providing resonance for 28 GHz frequency band, offered high radiation efficiency (>90%), and 13 dBi gain. Moreover, good beam steering performance was achieved with stable gain for different scanning angles (up to 50°). Same kind of configuration was utilized by [58]. The authors designed a dual-polarized chain-slot-shaped pattern on the metal frame of a smartphone. Dual polarization was realized by exciting the antenna elements from the center and top side. Measurement results showed that the designed antenna realized a gain in the range of 8–12.6 dBi for both polarizations.

A multi-layer linear phased array design for mm-wave 5G mobile terminals was presented in [59].The phased array was designed on a low-loss substrate. The array's single element consisted of a compact off-center dipole element having same arm length as shown in Fig. 2.12(a). One arm of the dipole element was connected to the feed line using a feeding aperture and 4-layers of conducting vias,

while the other arm was connected to the ground plane placed on the third layer as shown in Fig. 2.12(b). The designed dipole element offered end-fire radiation characteristics with a gain of 4.56 dBi. After designing single antenna element, two sub-arrays of eight antenna elements were placed at different sides of the mobile phone PCB for realize MIMO characteristics.

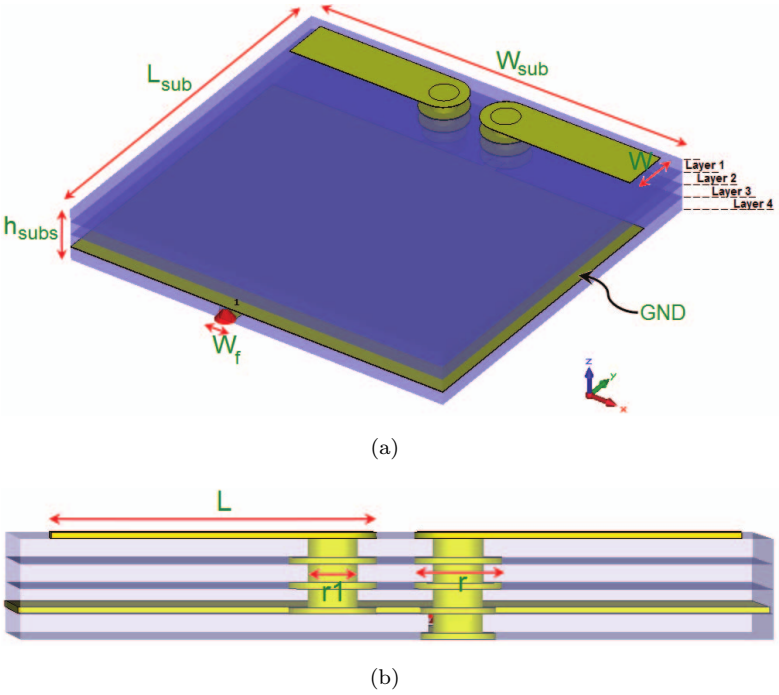

FIGURE 2.12: Geometry of single dipole element (a) perspective view and (b) side view [59].

In [60], a phased array of patch antennas was designed for 28 GHz mobile phone applications. The phased array consisted of three sub-arrays of eight patch elements, shown in Fig. 2.13, placed along on the edge of the smartphone PCB. The authors described that this kind of configuration lead to achieve broad 3D scanning coverage. Therefore, each sub-array had the ability to provide beam steering performance in the scanning range of $\pm 90^{\circ}$ with a gain of >10 dBi.

In [61], an 8-elements phased-array with end-fire radiation characteristics was designed for mm-wave wideband applications. The single element of the array was composed of a leaf-shaped bow-tie antenna as shown in Fig. 2.14. The designed antenna element offered an impedance bandwidth ranging from 25 GHz to 40

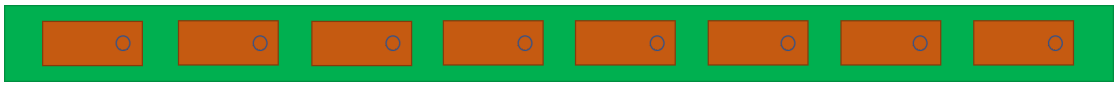

FIGURE 2.13: Patch Antenna Array for mm-wave mobile phone application [60].

GHz, which covers all the possible bands assigned for mm-wave mobile phone applications.

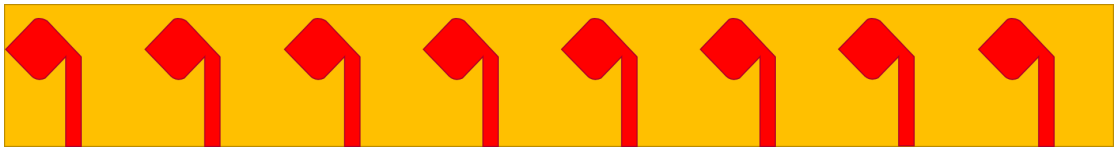

(a)

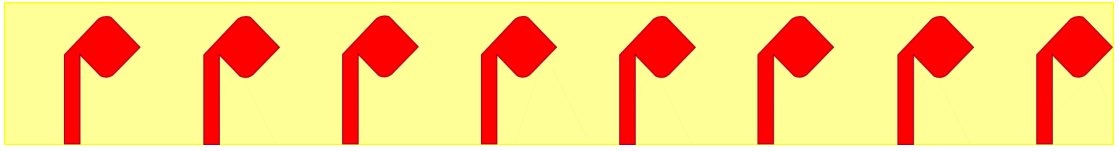

(b)

FIGURE 2.14: Design of the leaf-shaped bow-tie based phased array (a) front view and (b) back view [61].

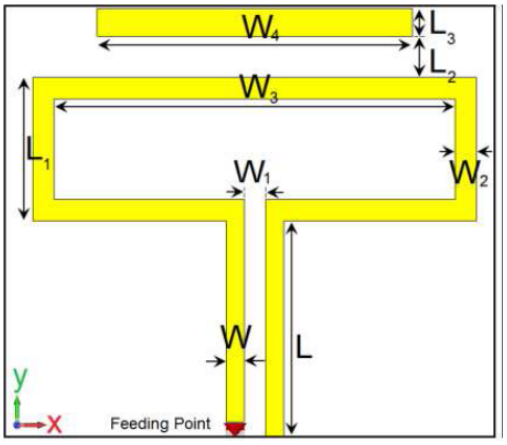

FIGURE 2.15: Schematic view of single antenna element showing folded-dipole and a single director [62].

Moreover, the designed antenna offered >97% radiation efficiency and almost stable gain of 4.5 dBi in the operating bandwidth. The performance of the phased array was checked by placing two sub-arrays at different sides of the mobile phone PCB, and observed a constant peak diversity of 10 dBi up to a scanning angle of 90°. In [63], a low-profile folded-dipole antenna based phased array was designed

with small clearance for mm-wave applications. The designed antenna element occupies only 0.5 mm space on the PCB. The radiation elements were etched from

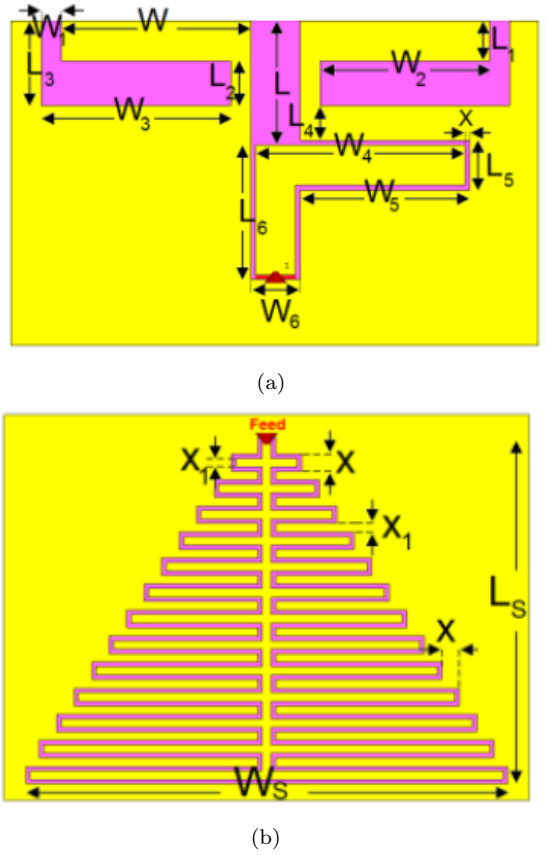

FIGURE 2.16: Schematic of the designed (a) CPW-fed dipole and (b) periodic slot elements [64].

the same layer as of ground plane. The presented phased array provided wide impedance bandwidth, high isolation of 20 dB, high efficiency, and beam steering over the wide scanning angles.

Same kind of phased array was designed in [62] with a single director for improved end-fire radiation characteristics. A schematic view of single antenna element is shown in Fig. 2.15. Moreover, the designed phased array provides ultra-wideband (UWB) response in the frequency range of 26–43 GHz. The use of director also enhanced the radiation efficiency of the antenna, which is ≈97%. In [64], the authors designed a dual-polarized phased array for 5G mm-wave applications. The phased array consisted of two sub-arrays, with each array of 8-elements: (a) a horizontally polarized CPW-fed dipole antennas, shown in Fig. 2.16(a) and

vertically polarized periodic slot antennas also shown in Fig. 2.16(b). The dipole elements resonate from 26.5 GHz to 39.5 GHz, while the periodic slot antennas resonate in the frequency range of 27.1–45.5 GHz. Moreover, both the sub-arrays had quasi end-fire radiation characteristics.

Table 2.2 presents a brief overview of previously proposed mm-wave MIMO antenna arrays.

TABLE 2.2: Brief overview of previously presented MIMO antenna arrays for mm-wave mobile phone applications.

Author	**Year**	**Development**	**Ref.**
Parchin et al.	2015	An air-filled slot-loop antenna array for 5G mobile phone applications.	[57]
Parchin et al.	2015	A multi-layer linear phased array design for mm-wave 5G mobile terminals.	[59]
Parchin et al.	2016	A phased array of patch antennas for 28 GHz mobile phone applications.	[60]
Parchin et al.	2016	An 8-elements phased-array design with end-fire radiation characteristics for mm-wave wideband applications.	[61]
Moreno et al.	2020	A dual-polarized chain-slot-shaped pattern antenna on the metal frame of a smartphone.	[58]
Parchin et al.	2020	A low-profile folded-dipole antenna-based phased array for mm-wave applications.	[63]
Parchin et al.	2021	A dual-polarized phased array for 5G mm-wave cellular communications.	[64]

2.3 Summary

This chapter presents a detailed discussion on previously presented MIMO antennas for sub-6 GHz and mm-wave 5G applications. The designs of planar and

non-planar MIMO antenna arrays specifically for sub-6 GHz 5G applications are discussed in detail along with their performance. In addition, the phased arrays, designed and developed for mm-wave applications are discussed in detail.

Chapter 3

Uni-Planar MIMO Antenna Array for Sub-6 GHz 5G Cellular Applications

For fifth-generation (5G) communication, most research societies are concentrating on obtaining high throughput and high data rates at a cheap cost [65, 66]. It is predicted that the 5G systems will have a data rate 1000 times faster compared with the fourth-generation (4G) communication systems. Such a high data rate can be achieved with the help of multiple-input multiple-output (MIMO) technology [67, 68].

In MIMO, the data rate can be improved by reducing multipath fading or by utilizing multiple independent channels. One of the major keys to boosting the channel capacity is to design several antennas for each channel [68]. The MIMO antenna must have a low mutual coupling, which is a prerequisite for a 5G mobile communication system [68]. Moreover, the 5G MIMO antennas can offer better diversity and multiplexing gain [69], which leads to enhanced channel capacity [70].

In the literature, several MIMO antennas have been presented for sub-6 GHz applications. In [36], an eight-element MIMO structure was developed for the 3.5

GHz spectrum. A symmetrical open-fork slit antenna with an L-shaped feeding strip was designed. This configuration offers isolation of >17.5 dB between antenna elements, but the design suffers because of poor antenna efficiency. The same kind of configuration with a rectangular-shaped slot was presented in Ref. [37]. The MIMO arrays consisted of two kinds of antenna elements for different frequency operations. Two elements of the same configuration were placed on the top and bottom corners of the printed circuit board (PCB) for 2G/3G/4G communication, while eight-elements meant to operate at 3.5 GHz were placed on the left and right sides of the PCB. The authors in [41] designed an eight-port broadband MIMO antenna for sub-6 GHz services. The single antenna of the MIMO system was made up of a 50 Ω feed line with an open circuit tuning stub, a slot on the metal frame, and a U-shaped slot on the ground plane. The MIMO antenna provided a broadband response in the frequency range of 3.3-6 GHz. In [30], a monopole slotted MIMO antenna was presented for the 2.6/3.5 GHz bands. The four metal frame-based antennas fed using an L-shaped feed line were positioned in the middle of the PCB, while the other elements were placed on the top and bottom sides of the PCB.

In [42], a MIMO antenna array was designed for 3.5 GHz 5G smartphone applications. The array was made up of two distinct ways: one was an L-shaped coupled-fed array and the other was a U-shaped loop array, both of which were mounted on the smartphone's metal frame. For isolation enhancement, the authors created an inverted-I slot and a neutralization line between the antenna components, resulting in 15 dB of isolation in the operational bandwidth. In [43], a dual-polarized diamond ring slot-based MIMO antenna was designed for 5G massive MIMO applications. Four dual-fed slot elements were placed on each corner of the mobile phone PCB. An L-shaped microstrip feed line was used to feed the slot elements. The designed antenna element offered a stable gain of 3 dBi for the band of interest and >80% radiation and total efficiencies. In addition, an isolation of more than 20 dB was observed within the operating range. In [44], the same kind of configuration was utilized to design MIMO antenna array for sub-6 GHz applications. In the presented configuration, a circular-ring resonator was

etched from the ground plane and fed using orthogonally placed microstrip feed lines. The authors also designed a multi-band MIMO antenna by replacing the conventional microstrip feed line with a fork-shaped feed line.

In [49], an eight-port MIMO antenna based on an I-shaped element was developed for IoT and 5G technologies. To provide space for additional components, the cell-phone's metal frame was constructed to accommodate the antenna components. The antenna was found to resonate effectively in the 3.5 GHz frequency band. The MIMO antenna offers 13 dB of isolation between array elements, with a gain of 4 dBi and an antenna efficiency of more than 40%. In [50], an integrated MIMO antenna system for LTE and millimeter-wave frequency bands was designed. The designed antenna structure comprised two elements for LTE communications and four elements for 5G millimeter-wave communication. A modified rectangular radiator was utilized for both frequency bands. In addition, defects in the ground plane were introduced using rectangular and circular shapes. The designed antenna element provides resonance for the 5.5 GHz frequency band. A uni-planar sub-6 GHz MIMO loop antenna array was developed in [51]. The antenna antennas were organized in such a way so that they could offer both polarization and pattern diversity. Furthermore, the improvement in isolation was achieved by designing an arrow-shaped strip between the antenna elements. In [53, 54], the authors designed a co-planar waveguide (CPW)-fed MIMO antenna array for sub-6 GHz applications. For the design, an L-shaped and T-shaped radiation elements were selected. By utilizing CPW technique, an isolation of >15 dB was achieved in the band of interest.

The abovementioned MIMO antennas have some limitations in terms of non-planar configurations, large size, and complex structures. In addition, these antennas suffer due to low radiation efficiency, which ultimately leads to poor antenna gain. To accommodate the drawbacks of previously published designs, this research presents a four-element uni-planar MIMO antenna system for 5G smartphone applications. For a single antenna, a loop-shaped element is chosen. The radiation elements are arranged at each corner of the PCB, which follows the principle of pattern diversity and makes room for other smartphone components. The results show that

the designed MIMO antenna offers wideband response in the 3.5 GHz frequency band. The intended MIMO topology has low mutual coupling between antennas, resulting in a low envelope correlation coefficient (ECC) and high diversity gain (DG). Moreover, the proposed MIMO antenna offers an efficiency of >90%.

3.1 Proposed Uni-Planar MIMO Antenna

The design of the proposed sub-6 GHz MIMO antenna is given in Fig. 3.1. A low-cost FR-4 substrate of thickness 1.6 mm having a relative permittivity of 4.4 is used for MIMO antenna design. To save space on the PCB, a loop-shaped structure was used for the antenna design [71].

At 3.5 GHz, the electrical length of a radiator is approximately equal to $1\lambda_g$, where λ_g is the guided wavelength and can be calculated as:

$$\lambda_g = \frac{c}{f_r\sqrt{\epsilon_{eff}}} \tag{3.1}$$

where

$$\epsilon_{eff} = \frac{\epsilon_r + 1}{2} \tag{3.2}$$

where, c is the speed of light, which is 3×10^8 m/s, f_r is the resonant frequency, and ϵ_r and ϵ_{eff} is the relative permittivity and effective relative permittivity of the dielectric substrate.

The optimized electrical length of an antenna element is ≈45.5 mm, while the line width is equal to 1 mm. It is worth noting that a single antenna element can occupy a maximum area of 14.5×12 mm^2.

The MIMO antenna, as shown in Fig. 3.1, comprised of four loop-shaped radiators placed at each corner of the mobile phone PCB. The ground plane is placed on the same plane as the radiation elements. The design parameters of the proposed MIMO antenna are illustrated in Fig. 3.1, while the optimized values are given in Table 3.1.

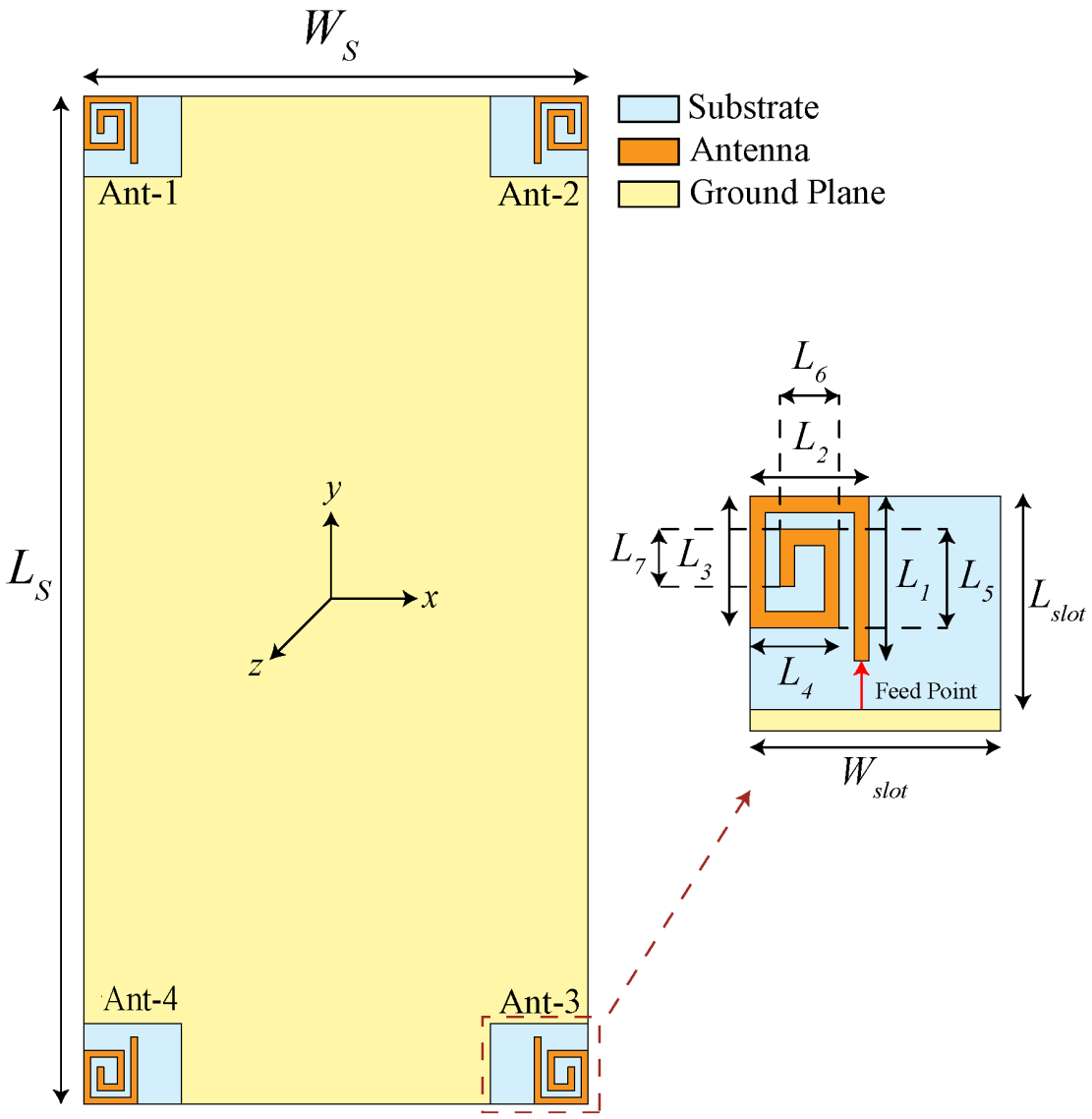

FIGURE 3.1: Configuration of the designed MIMO antenna.

TABLE 3.1: MIMO antenna's optimized design parameters (values in mm).

L_S	W_S	L_1	L_2	L_3	L_4	L_5	L_6	L_7	L_{slot}	W_{slot}
150	75	10	8	8	6	6	4	3.5	12	14.5

3.2 Characteristics of Single Antenna Element

The single MIMO element is designed and simulated in the commercially available electromagnetic software CST Microwave Studio. For the excitation of the antenna element, a 50Ω discrete port is utilized. Figure 3.2 shows the simulated reflection coefficient (S_{11}) of a single antenna element. It is observed that the antenna

element resonates well in the 3.5 GHz frequency band and also provides a wideband response. The -6 dB and -10 dB impedance bandwidths are noted to be 1.28 GHz (3–4.28 GHz) and 720 MHz (3.18–3.9 GHz), respectively.

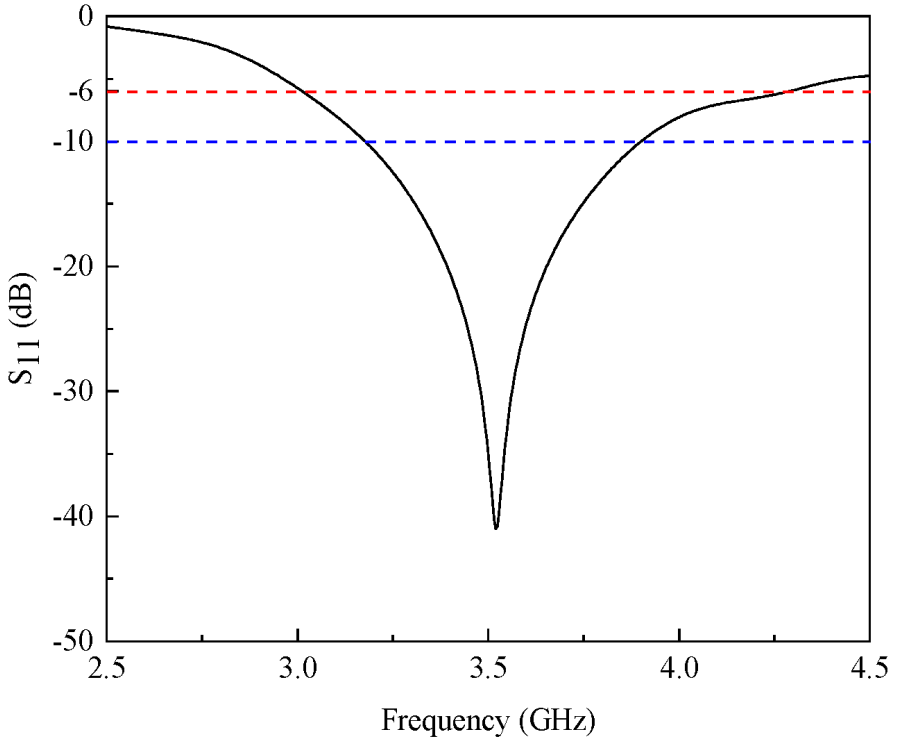

FIGURE 3.2: Simulated S_{11} characteristics of single antenna element.

The S_{11} of the proposed antenna can be adjusted by changing some parameters of the antenna. For a particular design, the parameters W_{slot} and L_{slot} have a great impact on the performance. The parameter W_{slot} plays a major role in achieving impedance matching in the band of interest, while the parameter L_{slot} can be tuned to obtain resonance for the desired frequency band. This effect is clearly visible in the results of Fig. 3.3, which shows the S_{11} characteristics of the designed antenna for varying W_{slot} and L_{slot}.

Figure 3.3(a) illustrates the S_{11} characteristics of the proposed antenna for varying values of parameter W_{slot}. It can be noted from the figure that the parameter W_{slot} has a significant effect on impedance matching. The maximum impedance matching is observed for W_{slot} = 14.5 mm as shown in Fig. 3.3(a). On the other hand, when the value of parameter L_{slot} is changed in the range of 11.5 mm to

14.5 mm, a shift in the resonant frequency is observed as shown in Fig. 3.3(b). It is important to mention here that these values have a negligible effect on the isolation performance of MIMO antennas.

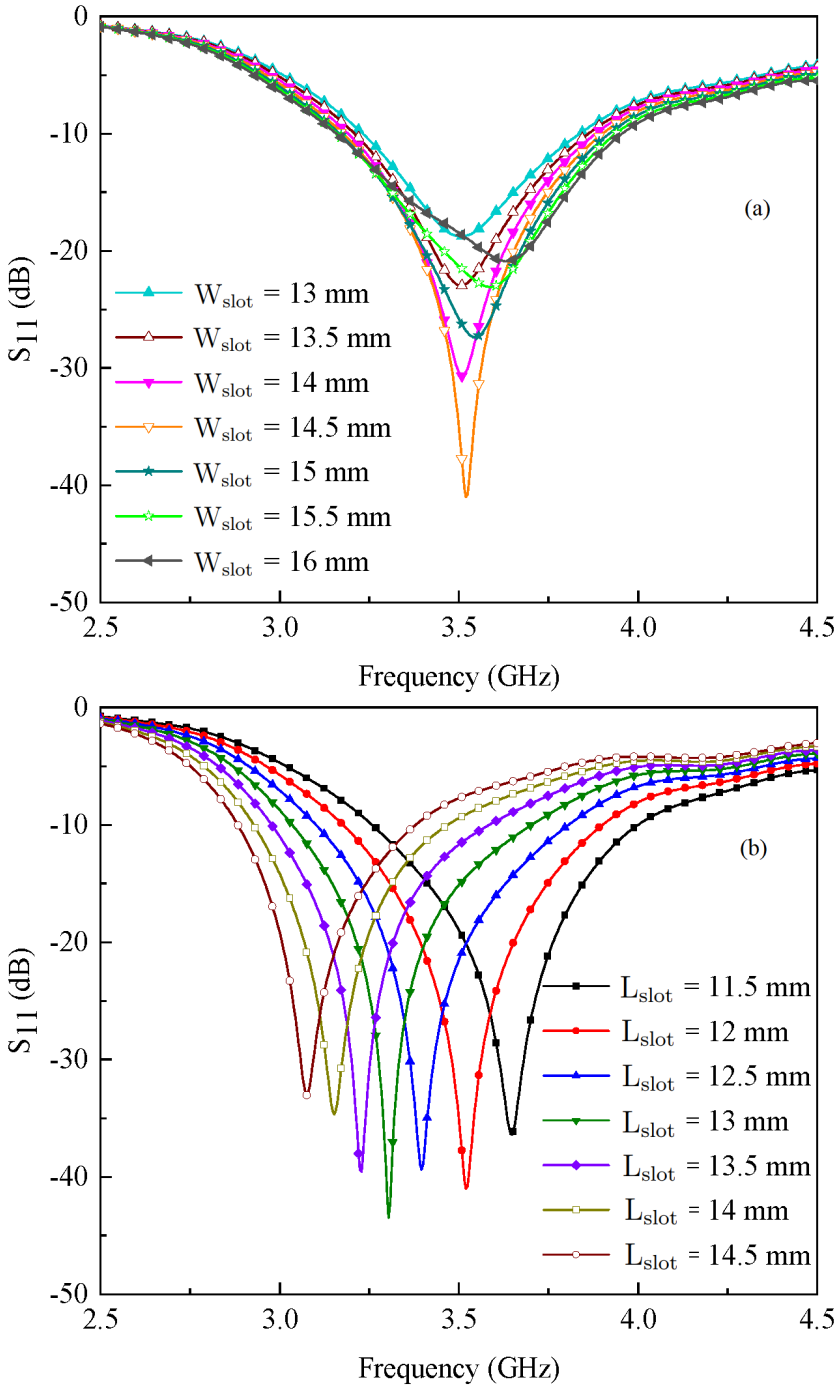

FIGURE 3.3: Simulated S_{11} characteristics for different values of (a) W_{slot} and (b) L_{slot}.

3.3 Characteristics of Proposed MIMO Array

The simulated S-parameters of the proposed MIMO antenna are shown in Fig. 3.4. It is observed from the simulated S-parameters that the designed MIMO antenna is resonating for the 3.5 GHz frequency band. Furthermore, the minimum isolation between closely spaced antennas is observed to be >10 dB. A variation is observed in the S_{11} response, which mainly occurred due to feeding points and different placements of antenna elements on the smartphone PCB, as shown in Fig. 3.1. In addition to this, the mainboard is rectangular in nature, which could cause some discrepancies in the frequency response and couplings, mainly between even and odd port numbers. However, one can adjust the desired frequency band by modifying design parameters explained in Fig. 3.3 [72].

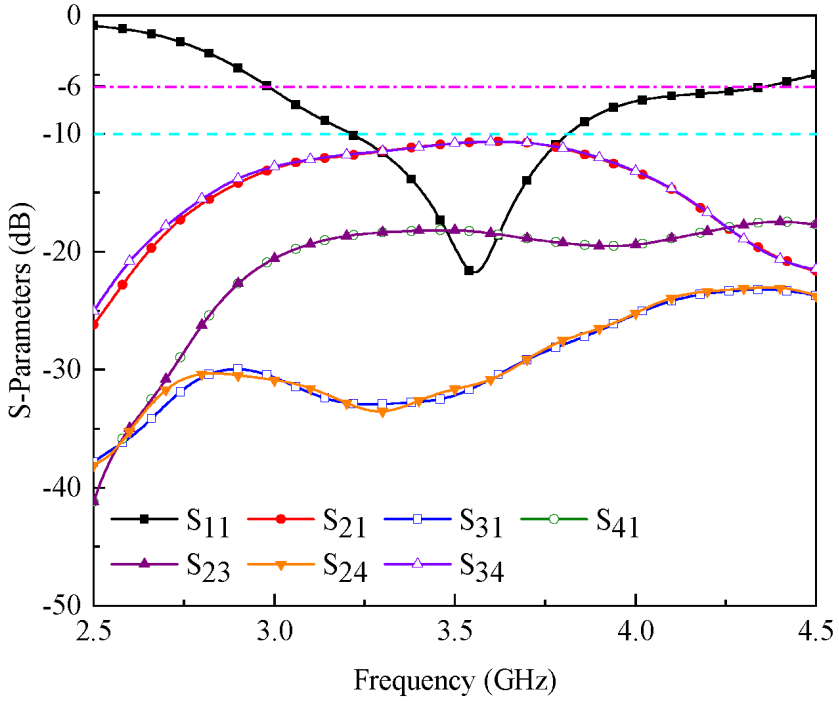

FIGURE 3.4: Simulated reflection coefficient and port isolation results of the proposed MIMO antenna.

The designed antenna simulated three-dimensional (3-D) gain patterns are presented in Fig. 3.5. The antenna generates different vertical and horizontal polarized radiation patterns for the chosen frequency band, as shown in the diagram. In addition, as demonstrated in Fig. 3.5, the antenna has a gain of ∼3.6 dBi. The

resulting radiation patterns further confirm that the MIMO antenna adheres to pattern diversity, which is a desirable feature for future smartphone applications.

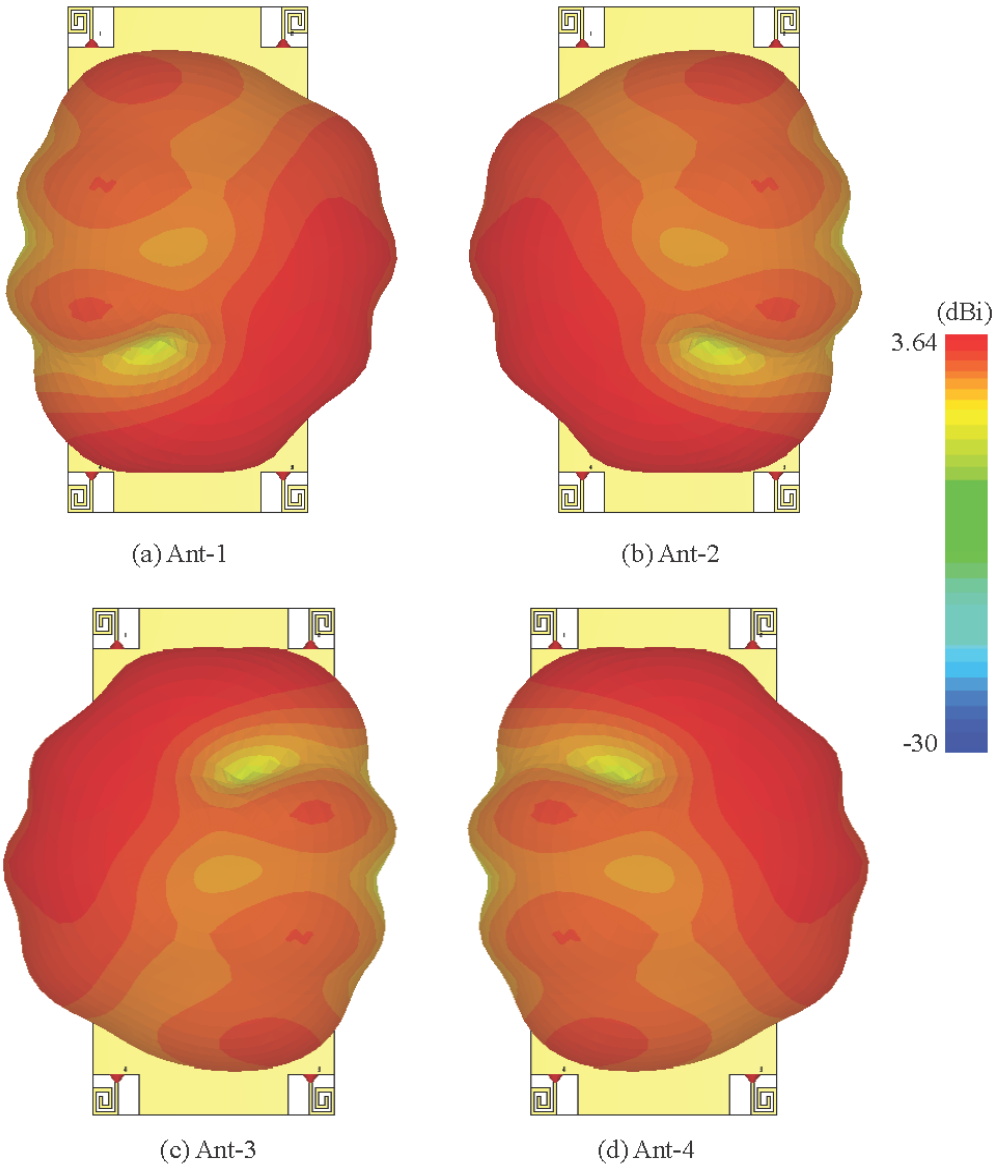

FIGURE 3.5: 3-D gain patterns of designed MIMO antenna.

One of the most critical aspects in determining the performance of MIMO antennas is the ECC. For practical applications, the ECC should be <0.5 and, idealy, it is ≈0. The ECC can be determined by using Eq. (1.4).

As shown in Fig. 3.6(a), the value of ECC for the intended frequency band (3.5 GHz) is <0.01. The results also demonstrate high isolation between antenna elements, which is a crucial factor for simultaneous operation.

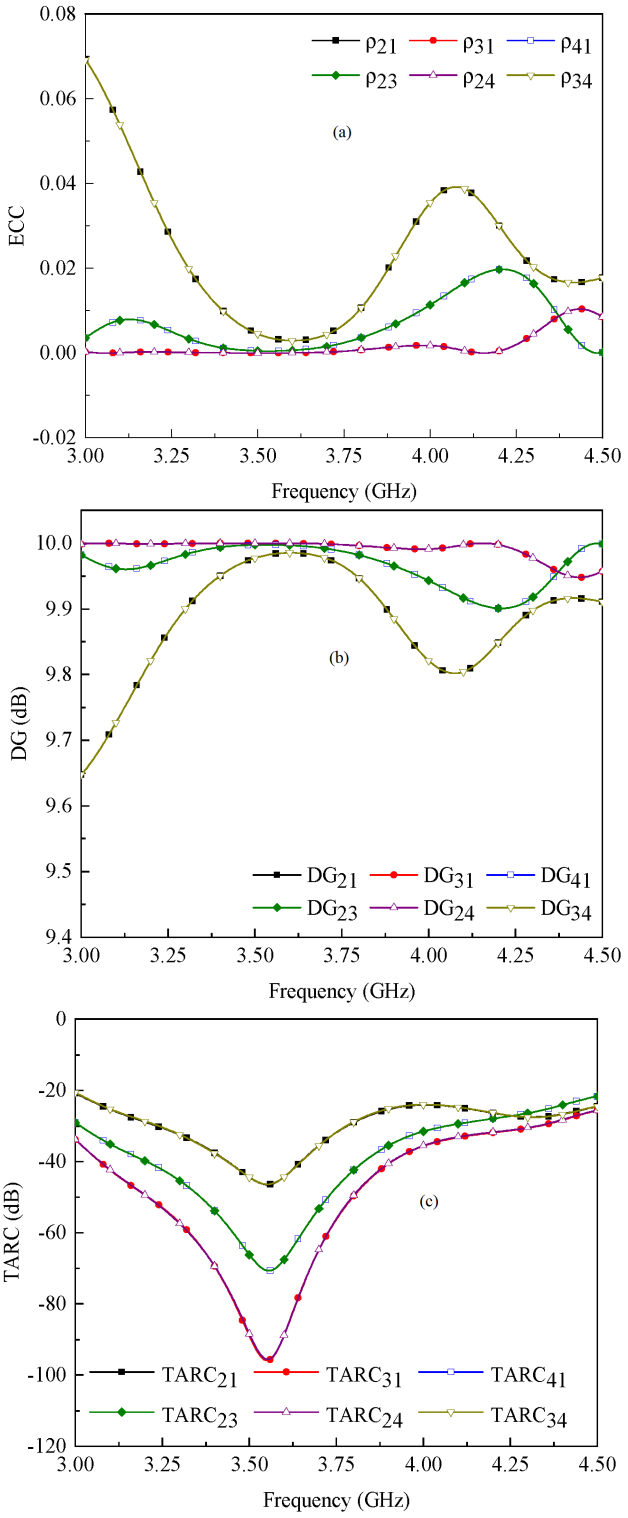

FIGURE 3.6: Simulated (a) ECC, (b) DG, and (c) TARC results of the proposed MIMO antenna.

The DG of the suggested MIMO antenna, on the other hand, can be calculated using Eq. (1.5). For the presented MIMO antenna, the DG value is noted to be >9.9 dB, as shown in Fig. 3.6(b).

The TARC is another significant metric to consider while evaluating the MIMO antenna's performance. It can be evaluated by using Eq. (1.8). The results demonstrate that the suggested MIMO antenna delivers TARC >20 dB for the band of interest, as illustrated in Fig. 3.6(c).

3.4 Fabrication and Measurements

A fabricated prototype of the proposed MIMO antenna is shown in Fig. 3.7 along with the feeding mechanism. The prototype if fabricated by using a milling machine. A flexible, semi-rigid RF cable is used for the feeding purpose. One end of the cable is connected to the antenna, while the second end is connected to a coaxial connector. Due to the similar performance and placement of the antenna elements, only port-1 and port-2 are measured and compared.

A comparison between simulated and measured S-parameters is given in Fig. 3.7. A reasonable agreement is observed between both S_{11} and S_{21}. The simulated -6 dB and -10 dB impedance bandwidths are noted to be 1.38 GHz (2.98–4.36 GHz) and 620 MHz (3.2–3.82 GHz), respectively; while the measured bandwidths are 1.45 GHz (2.96–4.41 GHz) and 680 MHz (3.13–3.81 GHz), respectively. Besides this, the isolation between antenna elements is >10 dB (see Fig. 3.7) at the desired frequency band.

Fig. 3.8 shows a comparison between simulated and measured ECC and TARC results. It is observed that the simulated and measured data are complying with each other. The ECC value for the band of interest is <0.08, as shown in Fig. 3.8(a). Aside from that, the TARC value for the operating band is 20 dB, as shown in Fig. 3.8(b).

The simulated and measured realized gain for port-1 is shown in Figure 3.9. The gain is measured by exciting port-1, while port-2 is terminated using a 50 Ω

(a)

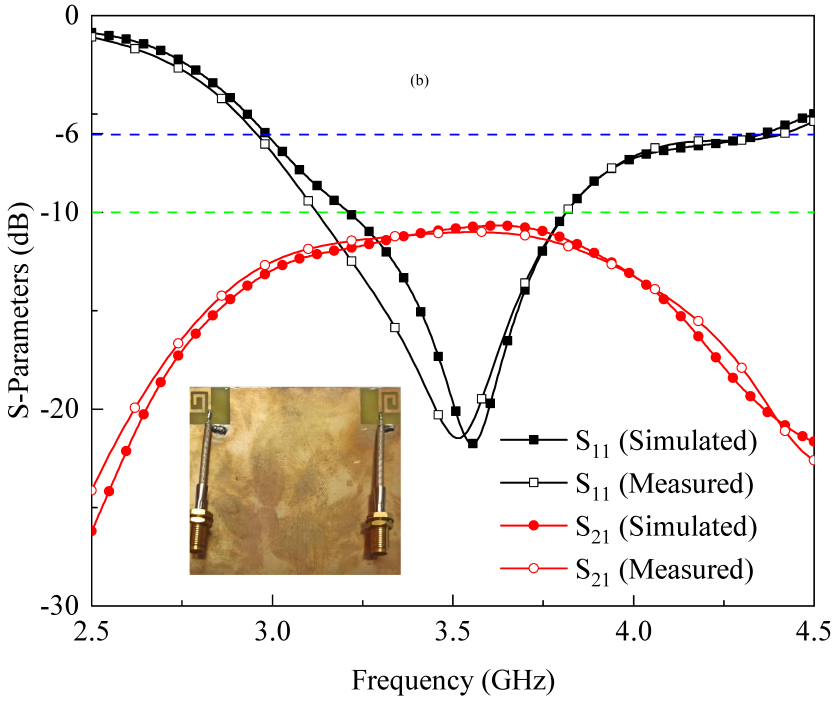

FIGURE 3.7: (a) Fabricated prototype of the proposed MIMO antenna. (b) Simulated and measured S-parameters of adjacent antenna elements (inset of the figure shows feeding mechanism of adjacent antenna elements).

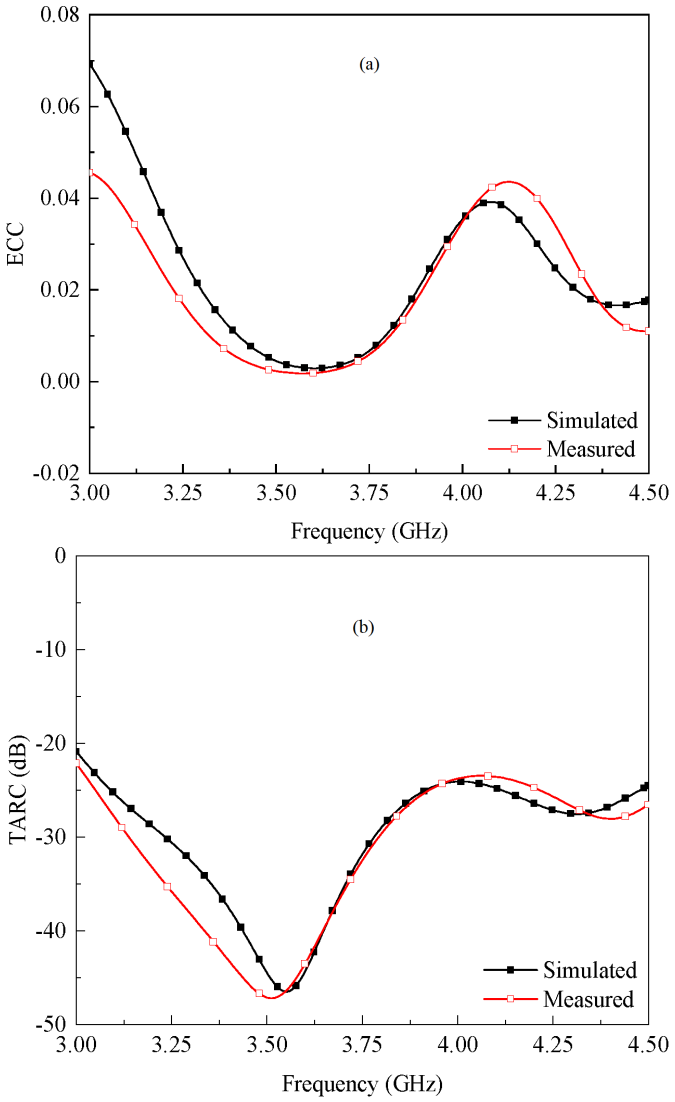

FIGURE 3.8: Simulated and measured (a) ECC and (b) TARC of adjacent antenna elements.

matched load. The average realized gain at port-1 is noted to be 4 dBi (see Figure 3.9). The simulated realized gain varies in the range from 2 to 4.75 dBi, while the measured value fluctuates in the range of 2.14–4.59 dBi, as shown in Figure 3.9.

The radiation and total efficiency for port-1 are shown in Figure 3.10. The MIMO antenna has a radiation efficiency >90%, while the total efficiency fluctuates in the range of 70–95%. One thing that needs to be observed from Figure 3.10 that the designed antenna offers constant radiation efficiency in the band of interest.

The simulated and measured radiation characteristics for port-1 and port-2 for

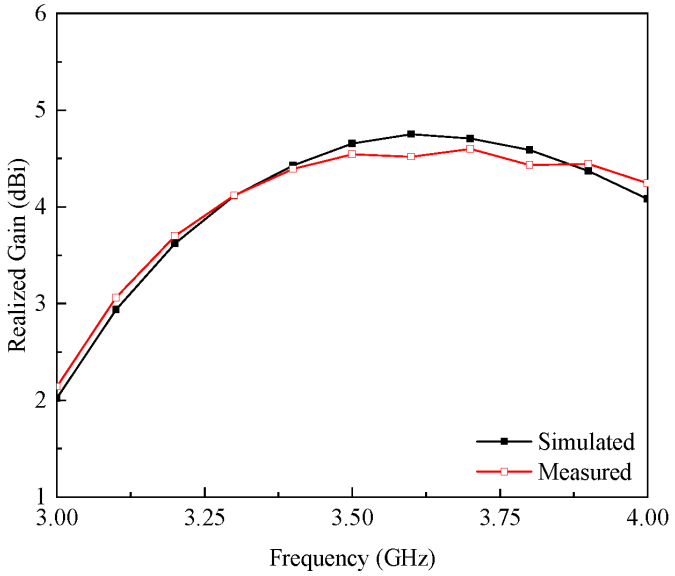

FIGURE 3.9: Simulated and measured realized gain of the proposed sub-6 GHz MIMO antenna when port-1 is excited.

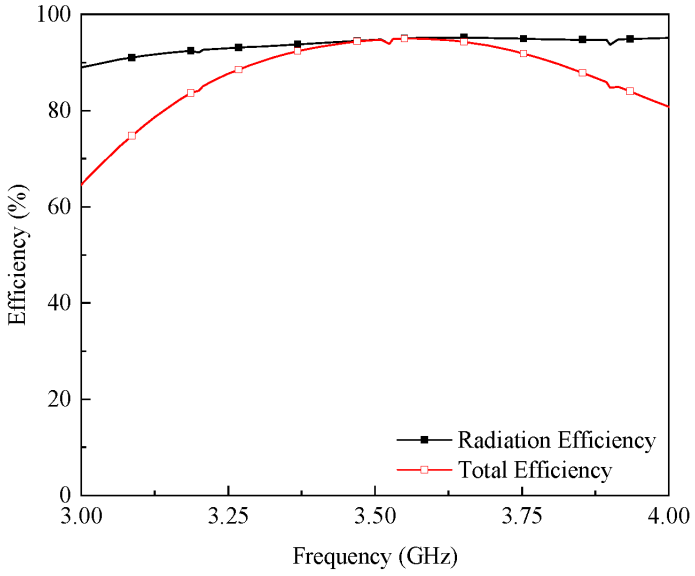

FIGURE 3.10: Simulated radiation and total efficiency of the proposed sub-6 GHz MIMO antenna when port-1 is excited.

frequencies 3.2 GHz, 3.5 GHz, and 3.9 GHz are illustrated in Figures 3.11 and 3.12. The designed MIMO antenna provides quasi-omnidirectional radiation characteristics for both yz- and xz-plane at the given frequencies.

In addition, the MIMO antenna offers pattern diversity in the xz-plane, as seen in Figures 3.11 and 3.12. Moreover, the measured results are well-matched with the simulated data for both planes.

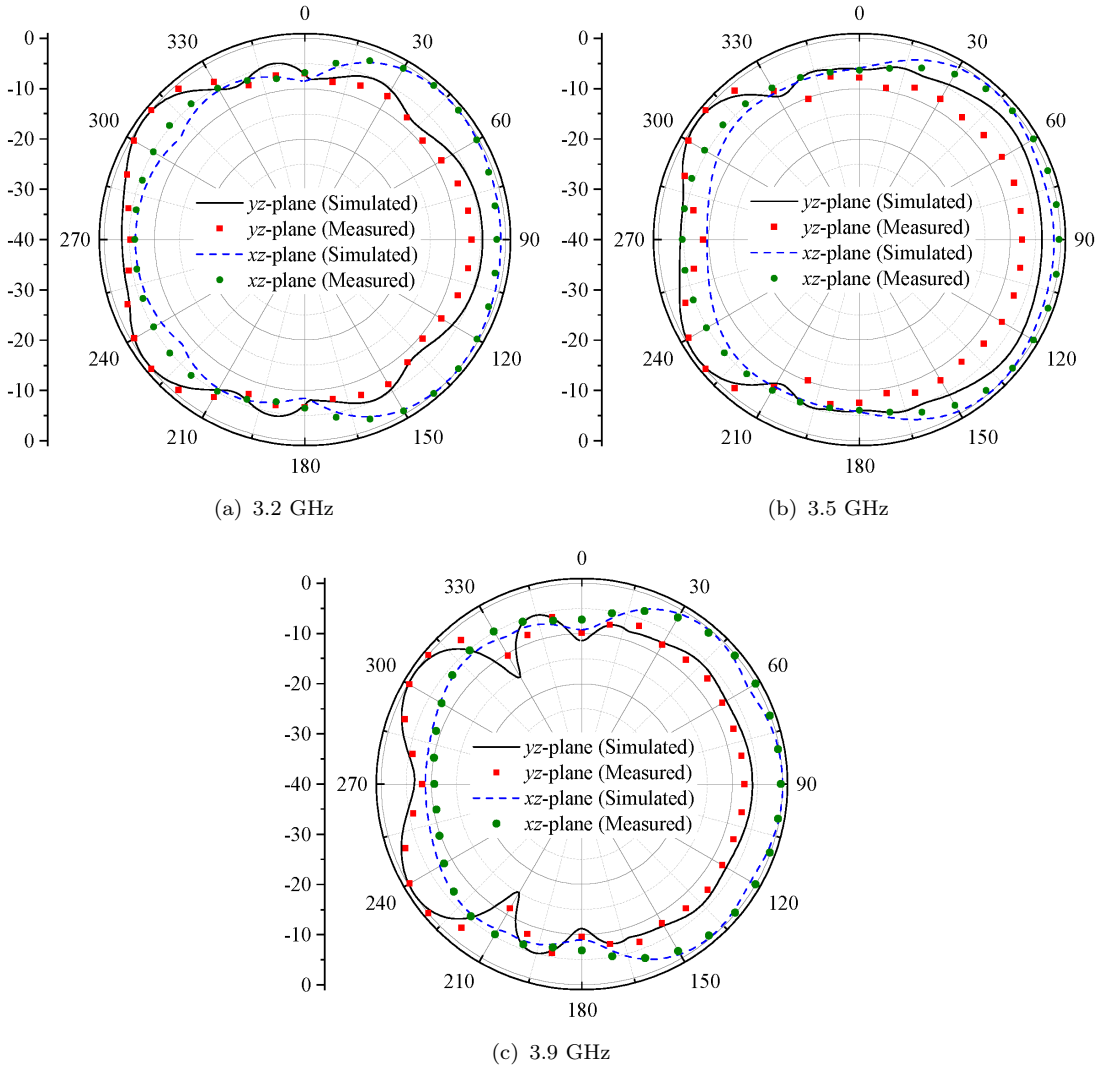

(a) 3.2 GHz

(b) 3.5 GHz

(c) 3.9 GHz

FIGURE 3.11: Radiation characteristics of the proposed sub-6 GHz MIMO antenna when port-1 is excited.

3.5 User Effect on Antenna Characteristics

In this section, the user's impact on MIMO antenna characteristics is examined. The performance is evaluated in terms of reflection coefficients, isolation between antenna elements, and radiation efficiency. The MIMO antenna performance is evaluated in the presence of the user's single and double hand, as shown in Figure 3.13(a, b).

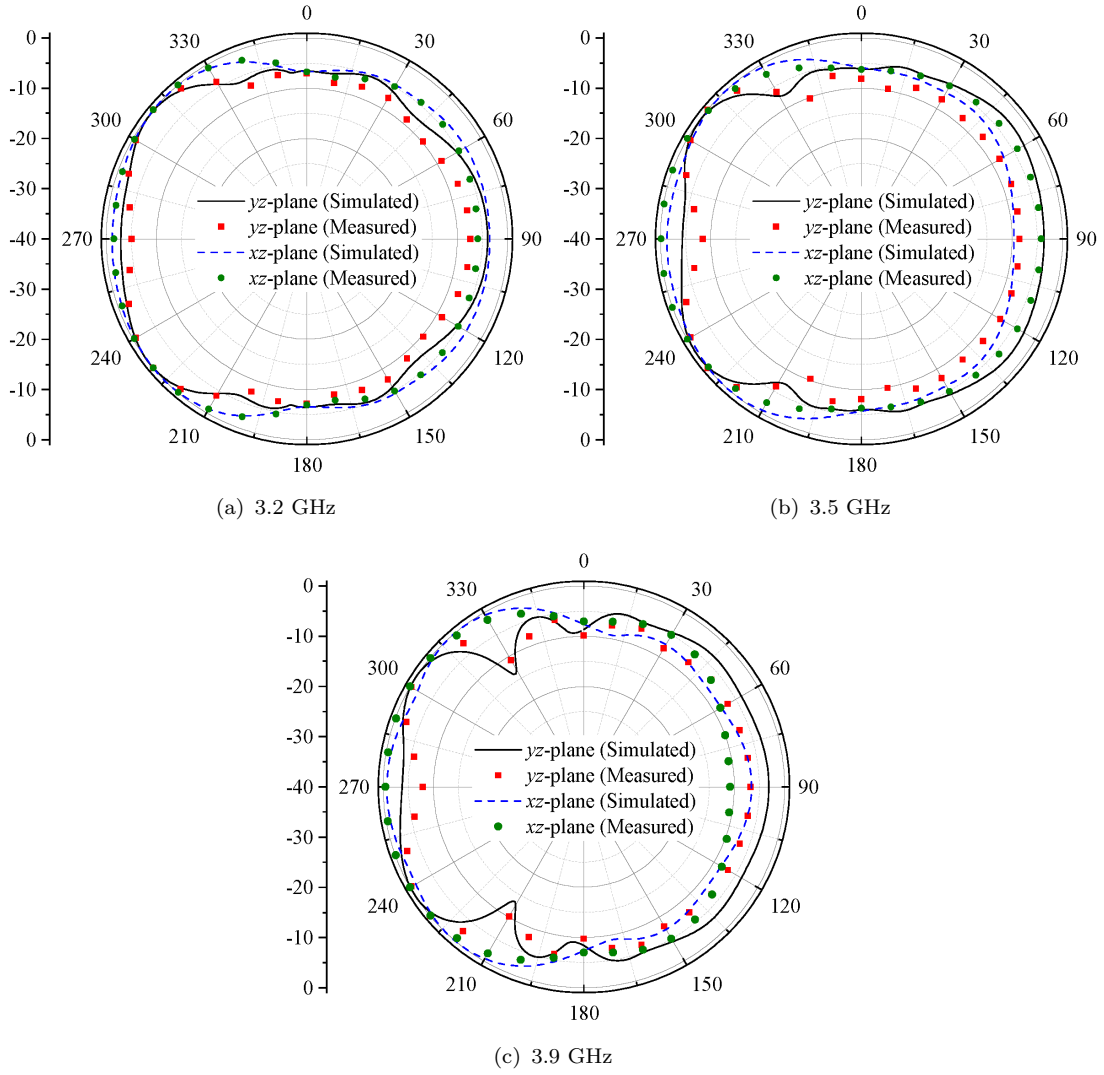

(a) 3.2 GHz

(b) 3.5 GHz

(c) 3.9 GHz

FIGURE 3.12: Radiation characteristics of the proposed sub-6 GHz MIMO antenna when port-2 is excited.

The developed MIMO antenna has appropriate reflection coefficients in the region of the human hands, as shown in Figure 3.14(a, b). For the single-hand scenario, >10 dB of isolation is noted between the antenna elements, as shown in Figure 3.15(a), while for double-hand mode, the isolation is >15 dB (see Figure 3.15b).

Besides this, from Figure 3.16(a, b), it can be noted that the efficiencies of antenna elements degraded. In case of single-handed operation, the reduction in radiation efficiency is noted for Ant-1 and Ant-3, whereas for the double-hand scenario, Ant-2 and Ant-3 provide less radiation efficiency. This is due to the features of human body tissue (fingers near the antenna), which can absorb a lot of antenna

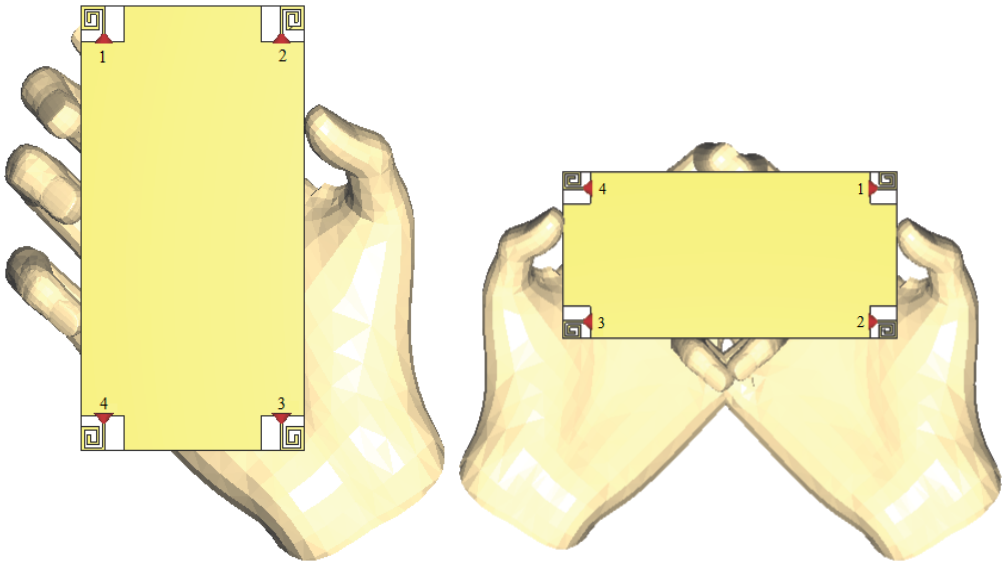

(a) (b)

FIGURE 3.13: MIMO array placement for (a) single-hand and (b) double-hand scenarios.

radiation power [73]. On the whole, the proposed MIMO antenna offers radiation efficiencies in the range of 39–68% for both scenarios for the desired frequency band.

For antennas used in mobile phone applications, one of the most important considerations is the specific absorption rate (SAR) [44, 60]. The SAR is a parameter that measures the amount of electromagnetic waves that are absorbed by the human body [74]. The SAR characteristics with user-head are explored and displayed in Fig. 3.17. The minimum and maximum SAR is noted to be 0.94 W/Kg for Ant-2 and 2 W/Kg for Ant-3, respectively. It is noted that the SAR value will be maximum if the antenna elements are closed to the head phantom.

A comparison of previously reported and designed sub-6 GHz MIMO antennas is given in Table 3.2. One can observe from the table that the electrical dimensions of the single antenna element are small compared to the designs of [36, 37, 43, 44]. The design presented in [42] offer high gain and low ECC, but due to their non-planar configuration, they can rarely be used in hand-held devices. On the other hand, the planar antennas designed in [36, 43, 44, 53] offer high isolation within

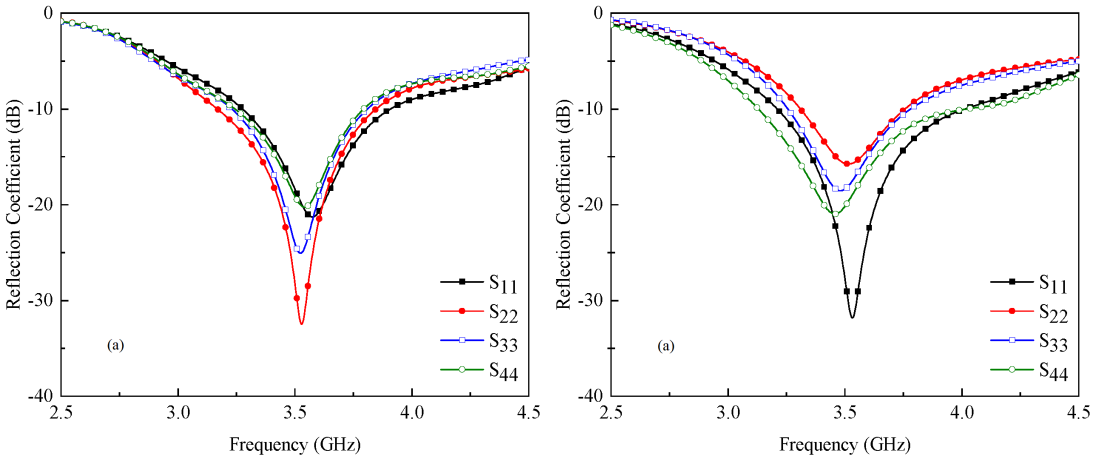

FIGURE 3.14: Reflection coefficients of MIMO antenna in case of (a) single-hand and (b) double-hand scenarios.

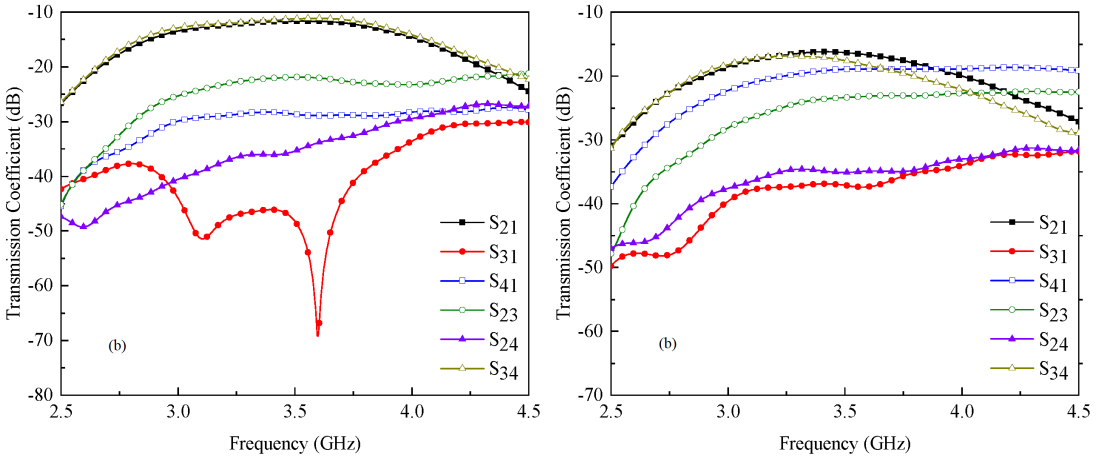

FIGURE 3.15: Transmission coefficients of MIMO antenna in case of (a) single-hand and (b) double-hand scenarios.

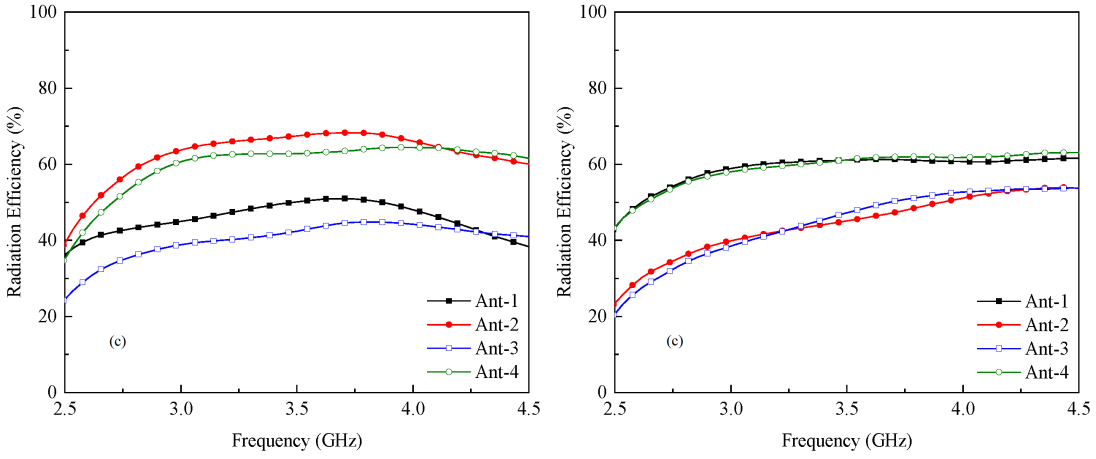

FIGURE 3.16: Radiation efficiency of MIMO antenna in case of (a) single-hand and (b) double-hand scenarios.

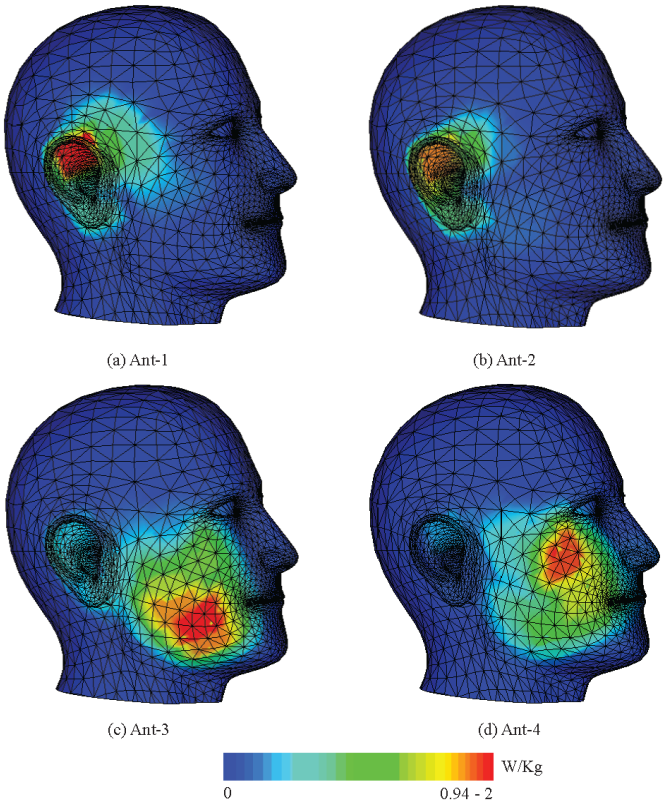

FIGURE 3.17: SAR analysis of MIMO antenna for talk-mode scenario.

their operational bandwidth, but they offer low antenna efficiency.

Therefore, it can be concluded from Table 3.2 that the proposed MIMO antenna offers high radiation efficiency, acceptable gain, and low ECC even with a lower number of elements.

TABLE 3.2: Comparison of proposed and previously reported sub-6 GHz MIMO antennas.

Ref.	Dimensions (mm^2)	Antenna Elements	Electrical Dimensions	Frequency Band (GHz)	Peak Gain (dBi)	Efficiency (%)	Isolation (dB)	ECC
[36]	150×80	8	0.239×0.128	3.4-3.6	–	>62	>17	<0.05
[37]	150×80	8	0.128×0.192	3.4-3.6	2-4	60-70	>10	<0.1
[30]	150×75	8	0.15×0.06	2.5-3.6	2.3	65	>13	<0.2
[42]	124×74	8	0.056×0.14	3.3-3.6	4.3-4.8	40	>15	<0.15
[43]	150×75	8	0.288×0.288	3.2-4	3	80	20	<0.01
[44]	150×75	8	0.291×0.291	3.3-3.9	3	60-80	18	<0.01
[49]	150×75	8	0.186×0.093	3.4-3.6	3.5-3.9	50-60	>13	<0.1
[51]	150×75	8	0.157×0.058	3.2-4	3.3-4	70-80	≥10	<0.005
[53]	150×75	8	0.24×0.038	3.4-4.4	3.6	>90	>16	<0.005
This Work	150×75	4	0.169×0.14	3.21-3.81	3.64	>90	>10	<0.02

3.6 Summary

A MIMO antenna design having uni-planar configuration is presented for sub-6 GHz 5G-enabled mobile phone applications. Four loop-shaped radiators are designed at each corner of a smartphone board, and they all follow the design configuration of pattern diversity. Several MIMO antenna features are evaluated, such as reflection coefficients, isolation between antenna elements, gain patterns, radiation and total efficiency, ECC, TARC, and DG. It can be concluded from the reported results that the presented MIMO antenna system successfully meets the criteria of 5G-enabled mobile phones.

Chapter 4

Phased Array Antenna for Millimeter-Wave 5G Mobile Phone Applications

5G-enabled handsets are planned to support mm-wave frequency bands in addition to the sub-6 GHz spectrum [55]. To fulfill the above-mentioned requirement, mobile phones are under experimentation with new antenna designs and their locations inside the device PCB. Furthermore, high-performance phased arrays are very desirable for mm-wave communication since they can improve the system's efficiency [75, 76] and be beneficial to overcome path loss effects.

In this chapter, the design of a compact 8-element linear phased array is designed for millimeter-wave 5G applications. To save space and cost, both the radiators and the ground plane are positioned on the same plane. To provide strong isolation between the antennas, a rectangular notch is designed on the ground plane. According to -6 dB bandwidth requirements, the phased array gives an impedance bandwidth of 8 GHz (24–32 GHz), while the impedance bandwidth is equal to 5 GHz (2530 GHz) for -10 dB bandwidth criteria. It is estimated that the isolation

between closely placed antenna elements is >15 dB. Moreover, the proposed array can beam steering characteristics for different scanning angles with omnidirectional radiation characteristics.

4.1 Design of Millimeter-Wave Phased Array

The design of a compact mm-wave phased array to be integrated onto a shared board is presented in this section. Figure 4.1(a) shows a schematic of the proposed phased array. The overall dimensions of the array are $W_a = 28$ mm and $L_a = 3.5$ mm. According to Fig. 4.1(a), the proposed array is made up of eight loop-type elements with resonant lengths of 1 λ_g at 28 GHz that are arranged in a linear pattern. A notch of 0.5×0.5 mm^2 is created in the ground plane to enhance isolation between the adjacent array elements. Moreover, each antenna element is fed separately using a 50Ω discrete port. The design of a single antenna element is illustrated in Fig. 4.1(b). The design parameters of the proposed array are as follows: $W_{ag} = 3$, $L_{ag} = 0.5$, $L_{a1} = 1.75$, $L_{a2}, L_{a3} = 1.5$, $L_{a4} = 0.85$, and $d = 2$ (all dimensions are in mm). The phased array is designed to operate at the 28 GHz frequency band, which is one of the most promising frequency bands for 5G applications [77, 78]. The designed phased array, however, is capable of covering other 5G bands, such as the 26 GHz and 30 GHz frequency bands, due to its broadband behavior [79–81].

4.2 Simulation Results and Discussion

Figure 4.2 depicts the simulated S-parameters of the proposed phased array. As can be seen, the designed phased array has a wide impedance bandwidth in the desired band. The observed -6 dB and -10 dB impedance bandwidths are 8 GHz (24–32 GHz) and 5 GHz (25–30 GHz), respectively. The isolation between adjacent antenna elements is >15 dB, shown in Fig. 4.2, for the entire operating bandwidth.

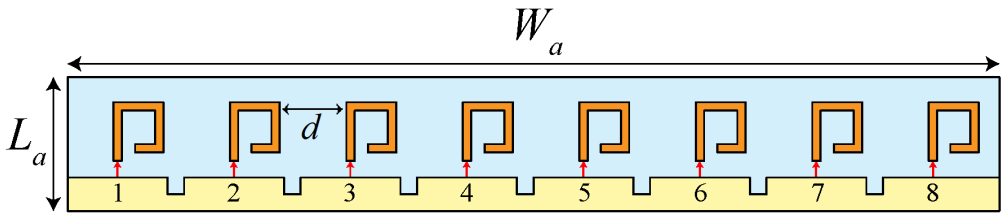

(a)

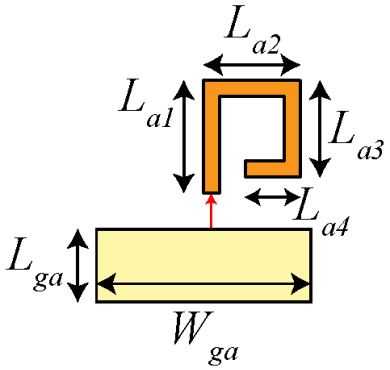

(b)

FIGURE 4.1: Schematic of the proposed (a) mm-wave phased array and (a) single antenna element.

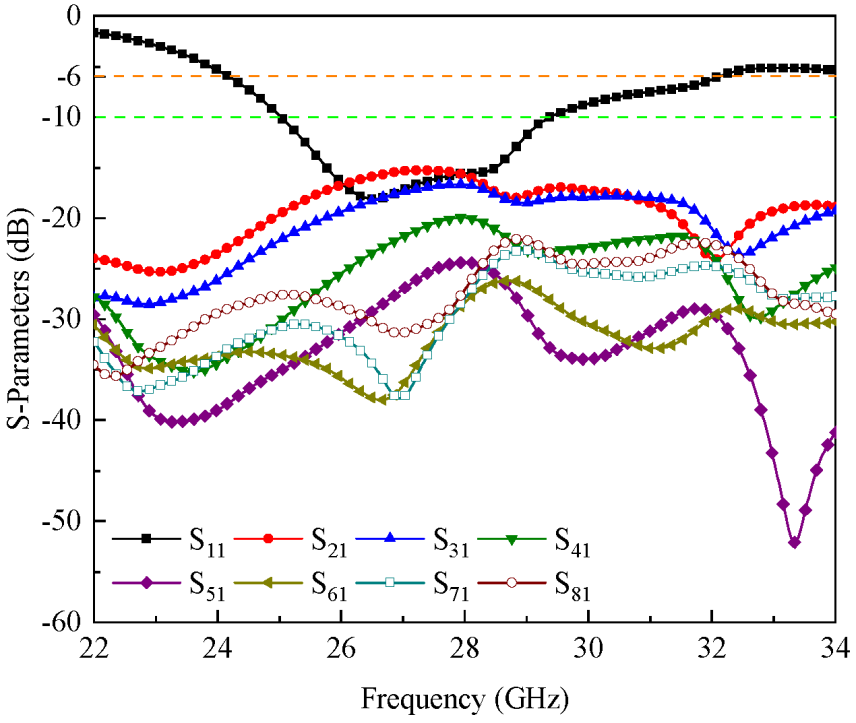

FIGURE 4.2: Simulated S-parameters of the proposed mm-wave phased array.

Figures 4.3 and 4.4 depict the 3-D and 2-D beam steering performance of the array for different scanning angles at 28 GHz. The direction and shape of the beams are observed by applying relative phase amplitudes to each array element according

to the following expression [82]:

$$\xi = 2\pi \left(\frac{d}{\lambda}\right) \sin\theta \tag{4.1}$$

where, d is the gap between array elements and θ represents the beam steering angle.

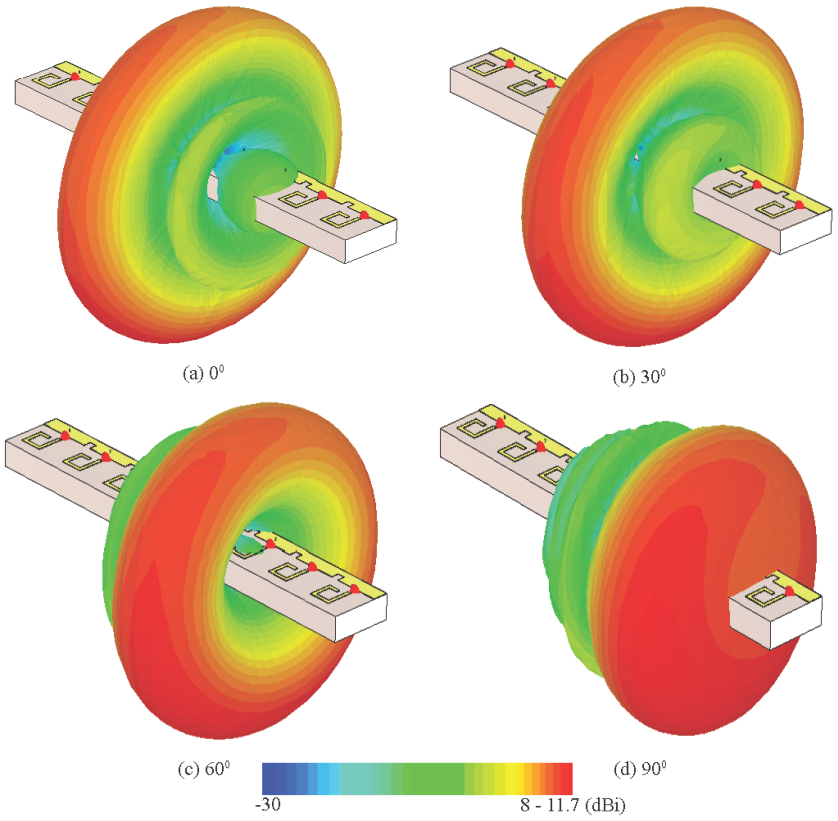

FIGURE 4.3: 3-D Beam steering performance of the proposed phased array for different scanning angles.

As shown in Fig. 4.3 and 4.4, the proposed phased array offers good beam steering performance with omni-directional radiation characteristics. It can also be observed from the result of Fig. 4.3 and 4.4 that the designed array exhibits high gain ($\approx$ 8–11.7 dBi) with low sidelobe levels (SLLs).

The Active Reflection Coefficients (ARCs) of the proposed phased array for different scanning angles are illustrated in Fig. 4.5(a). As the radiation beam of the antenna shifts towards a specific angle, the coupling between the radiation elements changes, which corresponds to the shift in ARC curves. The proposed

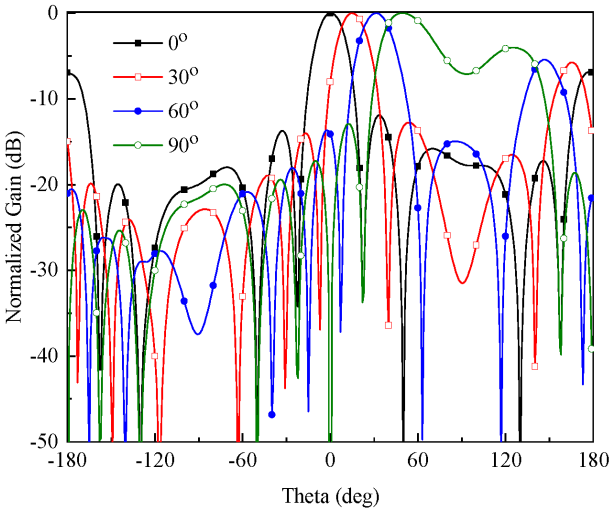

FIGURE 4.4: 2-D Beam steering performance of the proposed phased array for different scanning angles.

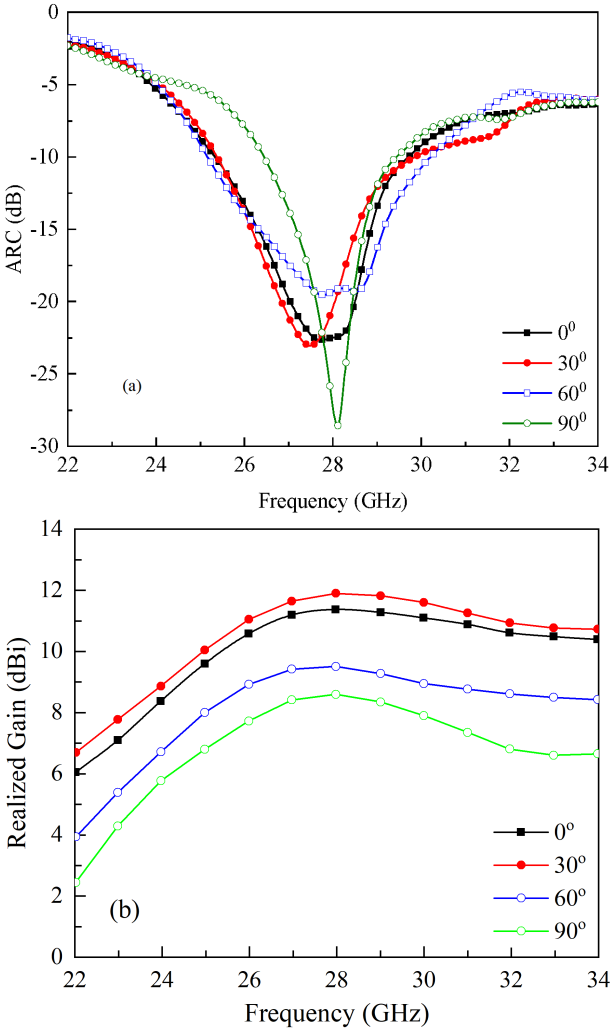

FIGURE 4.5: (a) Active reflection coefficient and (b) realized gain of the proposed mm-wave phased array for different scanning angles.

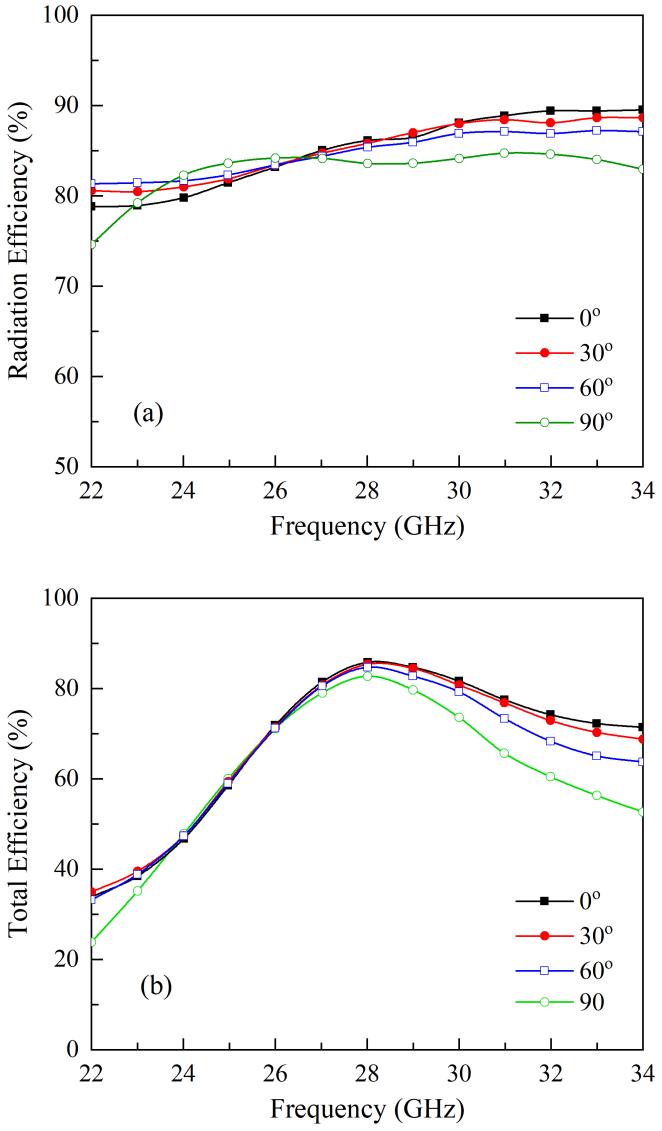

FIGURE 4.6: (a) Radiation and (b) total efficiency of the proposed mm-wave phased array for different scanning angles.

phased array exhibits sufficient ARC performance in the band of interest for different scanning angles as shown in Fig. 4.5(a).

Besides this, the realized gain curves for different scanning angles are depicted in Fig. 4.5(b). For 0° and 30°, the phased array offers a peak realized gain of 11.4 dBi, and 11.9 dBi, respectively, while for 60° and 90°, ∼2-3 dBi drop in gain value is observed due to the increase in Front-to-Back Ratio (FBR). Figure 4.6 shows the radiation efficiency and total efficiency of the proposed phased array for different scanning angels.

As observed, the phased array offers good efficiency results for the desired frequency band. The radiation (see Fig. 4.6a) and total efficiency (see Fig. 4.6b) vary in the range of 81.5–88.2% within the operating bandwidth.

4.3 Summary

This chapter presents phased array antenna design for mm-wave 5G applications. The designed array consists of eight loop-type elements arranged linearly on the smartphone board. For high isolation, a small notch is designed between the radiators. It is observed from the results that the designed phased array is resonating well in the 28 GHz frequency band and provides >15 dB of isolation between adjacent antenna elements. In addition, good beam steering performance is achieved with high gain and omni-directional radiation characteristics for a scanning angle up to 90°.

Chapter 5

Conclusion and Future Directions

5.1 Conclusion

With the development of 5G mobile communication standards, more research into related technologies is being performed to realize high transmission rates, lower cost, and higher gain. This can be achieved by using MIMO technology. The diversity approach can be used to generate numerous independent channels on the original spectrum using MIMO technology, and multipath fading can be decreased to increase the data transmission rate. As a result, MIMO antennas will be used in future mobile devices such as phones and tablets. Low-profile, wideband antenna elements with suitable mutual couplings are in high demand in 5G terminals for handheld device applications. Due to the limited size of the portable device, it is difficult to configure several antennas in such a constrained device.

A four-element MIMO antenna design for sub-6 GHz based systems is presented in this thesis. A uni-planar antenna configuration is used for the MIMO antenna array design. The array's single element is composed of a loop-type radiator placed at each corner of the smartphone PCB, which exhibits pattern diversity. It is described that the designed MIMO antenna resonates at the 3.5 GHz frequency band. From the presented results, it is demonstrated that according to $S_{11} \leq$ -6

dB threshold, the impedance bandwidth of the single antenna element is equal to 1.28 GHz (3–4.28 GHz), while for $S_{11} \leq$ -10 dB, it is equal to 720 MHz (3.18–3.9 GHz). Furthermore, a gain of >3.5 dBi and radiation efficiency >90% have been achieved. After evaluating the performance of a single antenna element, four elements are placed at each corner of the smartphone PCB. This configuration follows the principle of the pattern diversity technique. Through this configuration, an isolation of >10 dB is achieved between the antenna elements. The performance of the designed array is also accessed in the presence of a user and acceptable properties are observed in both data and talk mode.

This thesis also presents the design of a mm-wave phased array antenna. The designed phased array is able to provide a wideband response for the 28 GHz frequency band as well as beam steering performance with high gain.

5.2 Future Recommendations

The current research can be extended further into the following possible areas:

1. The number of elements can be extended to realize a massive MIMO antenna system for sub-6 GHz mobile phone applications, which can lead to enhanced gain and channel capacity.
2. For the enhancement of isolation between antenna elements, a decoupling structure can be utilized in the specified area on the PCB. This configuration can lead to achieving low ECC and high DG.
3. The proposed MIMO antenna's configuration can be used to achieve both polarization and pattern diversity.
4. The designed phased array for mm-wave applications provides omni-directional radiation characteristics. In the future, this phased array can be designed in such a manner that it will provide end-fire radiation properties.

Bibliography

[1] G. Gampala and C. Reddy, "Design of millimeter wave antenna arrays for 5G cellular applications using FEKO," in *2016 IEEE/ACES International Conference on Wireless Information Technology and Systems (ICWITS) and Applied Computational Electromagnetics (ACES)*, pp. 1–2, IEEE, 2016.

[2] G. Intelligence, "Definitive data and analysis for the mobile industry," *GSMAintelligence. com*, 2016.

[3] S. S. Sahoo, M. K. Hota, and K. K. Barik, "5G network a new look into the future: Beyond all generation networks," *American Journal of Systems and Software*, vol. 2, no. 4, pp. 108–112, 2014.

[4] A. F. Molisch, *Wireless communications*, vol. 34. John Wiley & Sons, 2012.

[5] I. Sector, "Requirements related to technical performance for IMT-advanced radio interface(s)," *Report ITU*, pp. 2134–2008, 2008.

[6] I. Poole, "LTE frequency bands and spectrum allocations," *Radio-Electronics. com: Resources and analysis for electronics engineers*, 2015.

[7] S. Parkvall, E. Englund, A. Furuskär, E. Dahlman, T. Jönsson, and A. Paravati, "LTE evolution towards IMT-advanced and commercial network performance," in *2010 IEEE International Conference on Communication Systems*, pp. 151–155, IEEE, 2010.

[8] E. Dahlman, G. Mildh, S. Parkvall, J. Peisa, J. Sachs, Y. Selén, and J. Sköld, "5G wireless access: requirements and realization," *IEEE Communications Magazine*, vol. 52, no. 12, pp. 42–47, 2014.

[9] Y. Wang, J. Li, L. Huang, Y. Jing, A. Georgakopoulos, and P. Demestichas, "5G mobile: Spectrum broadening to higher-frequency bands to support high data rates," *IEEE Vehicular Technology Magazine*, vol. 9, no. 3, pp. 39–46, 2014.

[10] W. Roh, J.-Y. Seol, J. Park, B. Lee, J. Lee, Y. Kim, J. Cho, K. Cheun, and F. Aryanfar, "Millimeter-wave beamforming as an enabling technology for 5G cellular communications: Theoretical feasibility and prototype results," *IEEE Communications Magazine*, vol. 52, no. 2, pp. 106–113, 2014.

[11] T. Kim, I. Bang, and D. K. Sung, "Design criteria on a mm-Wave based small cell with directional antennas," in *2014 IEEE 25th Annual International Symposium on Personal, Indoor, and Mobile Radio Communication (PIMRC)*, pp. 103–107, IEEE, 2014.

[12] E. Dahlman, G. Mildh, S. Parkvall, J. Peisa, J. Sachs, and Y. Selén, "5G radio access," *Ericsson review*, vol. 6, pp. 2–7, 2014.

[13] A. Osseiran, F. Boccardi, V. Braun, K. Kusume, P. Marsch, M. Maternia, O. Queseth, M. Schellmann, H. Schotten, H. Taoka, *et al.*, "Scenarios for 5G mobile and wireless communications: the vision of the metis project," *IEEE Communications Magazine*, vol. 52, no. 5, pp. 26–35, 2014.

[14] A. I. Sulyman, A. T. Nassar, M. K. Samimi, G. R. MacCartney, T. S. Rappaport, and A. Alsanie, "Radio propagation path loss models for 5G cellular networks in the 28 GHz and 38 GHz millimeter-wave bands," *IEEE Communications Magazine*, vol. 52, no. 9, pp. 78–86, 2014.

[15] R. A. Alhalabi, *High efficiency planar and RFIC-based antennas for millimeter-wave communication systems*. PhD thesis, UC San Diego, 2010.

[16] E. Dahlman, S. Parkvall, J. Sköld, and P. Beming, "3G evolution: HSPA and LTE for mobile broadband," 2008.

[17] A. Sibille, C. Oestges, and A. Zanella, *MIMO: From theory to implementation*. Academic Press, 2010.

[18] G. J. Foschini and M. J. Gans, "On limits of wireless communications in a fading environment when using multiple antennas," *Wireless Personal Communications*, vol. 6, no. 3, pp. 311–335, 1998.

[19] E. Telatar, "Capacity of multi-antenna Gaussian channels," *European Transactions on Telecommunications*, vol. 10, no. 6, pp. 585–595, 1999.

[20] W. C. Jakes and D. C. Cox, *Microwave mobile communications*. Wiley-IEEE Press, 1994.

[21] V. Pohl, V. Jungnickel, T. Haustein, and C. Von Helmolt, "Antenna spacing in MIMO indoor channels," in *IEEE 55th Vehicular Technology Conference*, vol. 2, pp. 749–753, IEEE, 2002.

[22] R. Vaughan, "Switched parasitic elements for antenna diversity," *IEEE Transactions on Antennas and Propagation*, vol. 47, no. 2, pp. 399–405, 1999.

[23] P. Mattheijssen, M. H. Herben, G. Dolmans, and L. Leyten, "Antenna-pattern diversity versus space diversity for use at handhelds," *IEEE Transactions on Vehicular Technology*, vol. 53, no. 4, pp. 1035–1042, 2004.

[24] L. Dong, H. Choo, R. W. Heath, and H. Ling, "Simulation of MIMO channel capacity with antenna polarization diversity," *IEEE Transactions on Wireless Communications*, vol. 4, no. 4, pp. 1869–1873, 2005.

[25] R. G. Vaughan and J. B. Andersen, "Antenna diversity in mobile communications," *IEEE Transactions on Vehicular Technology*, vol. 36, no. 4, pp. 149–172, 1987.

[26] P. Fletcher, M. Dean, and A. Nix, "Mutual coupling in multi-element array antennas and its influence on MIMO channel capacity," *Electronics Letters*, vol. 39, no. 4, pp. 342–344, 2003.

[27] M. K. Ozdemir, E. Arvas, and H. Arslan, "Dynamics of spatial correlation and implications on MIMO systems," *IEEE Communications Magazine*, vol. 42, no. 6, pp. S14–S19, 2004.

[28] S. Blanch, J. Romeu, and I. Corbella, "Exact representation of antenna system diversity performance from input parameter description," *Electronics Letters*, vol. 39, no. 9, pp. 705–707, 2003.

[29] P. Hallbjorner, "The significance of radiation efficiencies when using S-parameters to calculate the received signal correlation from two antennas," *IEEE Antennas and Wireless Propagation Letters*, vol. 4, pp. 97–99, 2005.

[30] M. Abdullah, S. H. Kiani, and A. Iqbal, "Eight element multiple-input multiple-output (MIMO) antenna for 5G mobile applications," *IEEE Access*, vol. 7, pp. 134488–134495, 2019.

[31] J. Yang, S. Pivnenko, T. Laitinen, J. Carlsson, and X. Chen, "Measurements of diversity gain and radiation efficiency of the eleven antenna by using different measurement techniques," in *Proceedings of the Fourth European Conference on Antennas and Propagation*, pp. 1–5, IEEE, 2010.

[32] A. Kumar, A. Q. Ansari, B. K. Kanaujia, and J. Kishor, "High isolation compact four-port MIMO antenna loaded with CSRR for multiband applications," *Frequenz*, vol. 72, no. 9-10, pp. 415–427, 2018.

[33] M. S. Sharawi, "Printed multi-band MIMO antenna systems and their performance metrics [wireless corner]," *IEEE Antennas and Propagation Magazine*, vol. 55, no. 5, pp. 218–232, 2013.

[34] D. M. Pozar, *Microwave engineering*. John wiley & sons, 2011.

[35] Y. Li, Y. Luo, G. Yang, *et al.*, "Multiband 10-antenna array for sub-6 GHz MIMO applications in 5-G smartphones," *IEEE Access*, vol. 6, pp. 28041–28053, 2018.

[36] Y. Li, Y. Luo, G. Yang, *et al.*, "High-isolation 3.5 GHz eight-antenna MIMO array using balanced open-slot antenna element for 5G smartphones," *IEEE Transactions on Antennas and Propagation*, vol. 67, no. 6, pp. 3820–3830, 2019.

[37] R. Ullah, S. Ullah, R. Ullah, F. Faisal, I. B. Mabrouk, and M. J. Al Hasan, "A 10-ports MIMO antenna system for 5G smart-phone applications," *IEEE Access*, vol. 8, pp. 218477–218488, 2020.

[38] L. Sun, H. Feng, Y. Li, and Z. Zhang, "Compact 5G MIMO mobile phone antennas with tightly arranged orthogonal-mode pairs," *IEEE Transactions on Antennas and Propagation*, vol. 66, no. 11, pp. 6364–6369, 2018.

[39] Z. Ren and A. Zhao, "Dual-band MIMO antenna with compact self-decoupled antenna pairs for 5G mobile applications," *IEEE Access*, vol. 7, pp. 82288–82296, 2019.

[40] Z. Ren, A. Zhao, and S. Wu, "MIMO antenna with compact decoupled antenna pairs for 5G mobile terminals," *IEEE Antennas and Wireless Propagation Letters*, vol. 18, no. 7, pp. 1367–1371, 2019.

[41] X. Zhang, Y. Li, W. Wang, and W. Shen, "Ultra-wideband 8-port MIMO antenna array for 5G metal-frame smartphones," *IEEE Access*, vol. 7, pp. 72273–72282, 2019.

[42] W. Jiang, B. Liu, Y. Cui, and W. Hu, "High-isolation eight-element MIMO array for 5G smartphone applications," *IEEE Access*, vol. 7, pp. 34104–34112, 2019.

[43] N. Ojaroudi Parchin, H. Jahanbakhsh Basherlou, M. Alibakhshikenari, Y. Ojaroudi Parchin, Y. I. Al-Yasir, R. A. Abd-Alhameed, and E. Limiti, "Mobile-phone antenna array with diamond-ring slot elements for 5G massive MIMO systems," *Electronics*, vol. 8, no. 5, p. 521, 2019.

[44] N. O. Parchin, Y. I. Al-Yasir, H. J. Basherlou, R. A. Abd-Alhameed, and J. M. Noras, "Orthogonally dual-polarised MIMO antenna array with pattern diversity for use in 5G smartphones," *IET Microwaves, Antennas & Propagation*, vol. 14, no. 6, pp. 457–467, 2020.

[45] A. Zhao and Z. Ren, "Size reduction of self-isolated MIMO antenna system for 5G mobile phone applications," *IEEE Antennas and Wireless Propagation Letters*, vol. 18, no. 1, pp. 152–156, 2018.

[46] A. Zhao, Z. Ren, and S. Wu, "Broadband MIMO antenna system for 5G operations in mobile phones," *International Journal of RF and Microwave Computer-Aided Engineering*, vol. 29, no. 10, p. e21857, 2019.

[47] A. Zhao and Z. Ren, "Multiple-input and multiple-output antenna system with self-isolated antenna element for fifth-generation mobile terminals," *Microwave and Optical Technology Letters*, vol. 61, no. 1, pp. 20–27, 2019.

[48] H. Wang, R. Zhang, Y. Luo, and G. Yang, "Compact eight-element antenna array for triple-band MIMO operation in 5G mobile terminals," *IEEE Access*, vol. 8, pp. 19433–19449, 2020.

[49] S. H. Kiani, A. Altaf, M. Abdullah, F. Muhammad, N. Shoaib, M. R. Anjum, R. Damaševičius, and T. Blažauskas, "Eight element side edged framed MIMO antenna array for future 5G smart phones," *Micromachines*, vol. 11, no. 11, p. 956, 2020.

[50] S. Iffat Naqvi, N. Hussain, A. Iqbal, M. Rahman, M. Forsat, S. S. Mirjavadi, and Y. Amin, "Integrated LTE and millimeter-wave 5G MIMO antenna system for 4G/5G wireless terminals," *Sensors*, vol. 20, no. 14, p. 3926, 2020.

[51] N. O. Parchin, H. J. Basherlou, Y. I. Al-Yasir, and R. A. Abd-Alhameed, "A broadband multiple-input multiple-output loop antenna array for 5G cellular communications," *AEU-International Journal of Electronics and Communications*, vol. 127, p. 153476, 2020.

[52] N. Ojaroudi Parchin, H. Jahanbakhsh Basherlou, and R. A. Abd-Alhameed, "Design of multi-mode antenna array for use in next-generation mobile handsets," *Sensors*, vol. 20, no. 9, p. 2447, 2020.

[53] N. Ojaroudi Parchin, H. Jahanbakhsh Basherlou, Y. I. Al-Yasir, A. M. Abdulkhaleq, M. Patwary, and R. A. Abd-Alhameed, "A new CPW-fed diversity antenna for MIMO 5G smartphones," *Electronics*, vol. 9, no. 2, p. 261, 2020.

[54] N. O. Parchin, Y. I. Al-Yasir, A. M. Abdulkhaleq, H. J. Basherlou, A. Ullah, and R. A. Abd-Alhameed, "A new broadband MIMO antenna system for sub 6 GHz 5G cellular communications," in *2020 14th European Conference on Antennas and Propagation (EuCAP)*, pp. 1–4, IEEE, 2020.

[55] T. S. Rappaport, S. Sun, R. Mayzus, H. Zhao, Y. Azar, K. Wang, G. N. Wong, J. K. Schulz, M. Samimi, and F. Gutierrez, "Millimeter wave mobile communications for 5G cellular: It will work!," *IEEE Access*, vol. 1, pp. 335–349, 2013.

[56] W. Hong, K. Baek, Y. Lee, and Y. G. Kim, "Design and analysis of a low-profile 28 GHz beam steering antenna solution for future 5G cellular applications," in *2014 IEEE MTT-S International Microwave Symposium (IMS2014)*, pp. 1–4, IEEE, 2014.

[57] N. Ojaroudiparchin, M. Shen, and G. F. Pedersen, "A 28 GHz FR-4 compatible phased array antenna for 5G mobile phone applications," in *2015 International symposium on Antennas and propagation (ISAP)*, pp. 1–4, IEEE, 2015.

[58] R. M. Moreno, J. Kurvinen, J. Ala-Laurinaho, A. Khripkov, J. Ilvonen, J. van Wonterghem, and V. Viikari, "Dual-polarized mm-wave endfire chain-slot antenna for mobile devices," *IEEE Transactions on Antennas and Propagation*, vol. 69, no. 1, pp. 25–34, 2020.

[59] N. Ojaroudiparchin, M. Shen, G. Fr, *et al.*, "Multi-layer 5G mobile phone antenna for multi-user MIMO communications," in *2015 23rd Telecommunications Forum Telfor (TELFOR)*, pp. 559–562, IEEE, 2015.

[60] N. Ojaroudiparchin, M. Shen, S. Zhang, and G. F. Pedersen, "A switchable 3-D-coverage-phased array antenna package for 5G mobile terminals," *IEEE Antennas and Wireless Propagation Letters*, vol. 15, pp. 1747–1750, 2016.

[61] N. O. Parchin, M. Shen, and G. F. Pedersen, "End-fire phased array 5G antenna design using leaf-shaped bow-tie elements for 28/38 GHz MIMO applications," in *2016 IEEE International Conference on Ubiquitous Wireless Broadband (ICUWB)*, pp. 1–4, IEEE, 2016.

[62] N. O. Parchin, Y. I. Al-Yasir, and R. A. Abd-Alhameed, "A compact 5G antenna array with ultra-wide bandwidth for mm-wave smartphone applications," in *2021 15th European Conference on Antennas and Propagation (EuCAP)*, pp. 1–4, IEEE, 2021.

[63] N. O. Parchin, H. J. Basherlou, Y. I. Al-Yasir, A. Ullah, A. A. Alabdullah, M. B. Melha, and R. A. Abd-Alhameed, "Small-clearance phased array antenna design with miniaturized elements for 5G communications," in *IMDC-SDSP 2020: Proceedings of the 1st International Multi-Disciplinary Conference Theme: Sustainable Development and Smart Planning, IMDC-SDSP 2020, Cyperspace, 28-30 June 202*, vol. 13, p. 139, European Alliance for Innovation, 2020.

[64] N. O. Parchin, J. Zhang, R. A. Abd-Alhameed, G. F. Pedersen, and S. Zhang, "A planar dual-polarized phased array with broad bandwidth and quasi end-fire radiation for 5G mobile handsets," *IEEE Transactions on Antennas and Propagation*, 2021.

[65] A. Osseiran, F. Boccardi, V. Braun, K. Kusume, P. Marsch, M. Maternia, O. Queseth, M. Schellmann, H. Schotten, H. Taoka, *et al.*, "Scenarios for 5G mobile and wireless communications: The vision of the METIS project," *IEEE Communications Magazine*, vol. 52, no. 5, pp. 26–35, 2014.

[66] A. Kammoun, M. Debbah, M.-S. Alouini, *et al.*, "Design of 5G full dimension massive MIMO systems," *IEEE Transactions on Communications*, vol. 66, no. 2, pp. 726–740, 2017.

[67] H. H Yang, *Massive MIMO meets small cell*. Springer, 2017.

[68] N. Ojaroudi Parchin, H. Jahanbakhsh Basherlou, Y. I. Al-Yasir, R. A. Abd-Alhameed, A. M. Abdulkhaleq, and J. M. Noras, "Recent developments of

reconfigurable antennas for current and future wireless communication systems," *Electronics*, vol. 8, no. 2, p. 128, 2019.

[69] J. G. Andrews, S. Buzzi, W. Choi, S. V. Hanly, A. Lozano, A. C. Soong, and J. C. Zhang, "What will 5G be?," *IEEE Journal on Selected Areas in Communications*, vol. 32, no. 6, pp. 1065–1082, 2014.

[70] N. O. Parchin, Y. I. A. Al-Yasir, and R. A. Abd-Alhameed, *Microwave/RF components for 5G front-end systems*. Avid Science, 2019.

[71] U. Ahmad, S. Ullah, U. Rafique, D.-Y. Choi, R. Ullah, B. Kamal, and A. Ahmad, "Mimo antenna system with pattern diversity for sub-6 GHz mobile phone applications," *IEEE Access*, vol. 9, pp. 149240–149249, 2021.

[72] Y. I. AI-Yasir, N. O. Parchin, A. Alabdullah, W. Mshwat, A. Ullah, and R. Abd-Alhameed, "New pattern reconfigurable circular disk antenna using two PIN diodes for WiMax/WiFi (IEEE 802.11a) applications," in *2019 16th International Conference on Synthesis, Modeling, Analysis and Simulation Methods and Applications to Circuit Design (SMACD)*, pp. 53–56, IEEE, 2019.

[73] M. Stuchly, "Electromagnetic fields and health," *IEEE Potentials*, vol. 12, no. 2, pp. 34–39, 1993.

[74] J. Moustafa, N. McEwan, R. Abd-Alhameed, and P. Excell, "Low SAR phased antenna array for mobile handsets," *Applied Computational Electromagnetics Society Journal*, vol. 21, no. 3, p. 196, 2006.

[75] N. O. Parchin, R. A. Abd-Alhameed, and M. Shen, "Frequency-switchable patch antenna with parasitic ring load for 5G mobile terminals," in *2019 International Symposium on Antennas and Propagation (ISAP)*, pp. 1–3, IEEE, 2019.

[76] N. Ojaroudi Parchin, M. Alibakhshikenari, H. Jahanbakhsh Basherlou, R. A Abd-Alhameed, J. Rodriguez, and E. Limiti, "MM-wave phased array

quasi-yagi antenna for the upcoming 5G cellular communications," *Applied Sciences*, vol. 9, no. 5, p. 978, 2019.

[77] N. O. Parchin, Y. Al-Yasir, A. M. Abdulkhaleq, I. Elfergani, A. Rayit, J. M. Noras, J. Rodriguez, and R. A. Abd-Alhameed, "Frequency reconfigurable antenna array for mm-Wave 5G mobile handsets," in *International Conference on Broadband Communications, Networks and Systems*, pp. 438–445, Springer, 2018.

[78] N. O. Parchin, M. Shen, and G. F. Pedersen, "Wideband Fabry-Pérot resonator for 28 GHz applications," in *2016 IEEE International Conference on Ubiquitous Wireless Broadband (ICUWB)*, pp. 1–4, IEEE, 2016.

[79] R. Li, Q. Zhang, Y. Kuang, X. Chen, Z. Xiao, and J. Zhang, "Design of a miniaturized antenna based on split ring resonators for 5G wireless communications," in *2019 Cross Strait Quad-Regional Radio Science and Wireless Technology Conference (CSQRWC)*, pp. 1–4, IEEE, 2019.

[80] D. Liu and B. Gaucher, "Design considerations for millimeter wave antennas within a chip package," in *2007 International Workshop on Anti-Counterfeiting, Security and Identification (ASID)*, pp. 13–17, IEEE, 2007.

[81] N. Ojaroudiparchin, M. Shen, and G. F. Pedersen, "Investigation on the performance of low-profile insensitive antenna with improved radiation characteristics for the future 5G applications," *Microwave and Optical Technology Letters*, vol. 58, no. 9, pp. 2148–2151, 2016.

[82] A. S. Abdullah, H. A. Al-Behadili, A. M. Abdulkhaleq, N. Ojaroudi Parchin, Y. I. Al-Yasir, R. A. Abd-Alhameed, and B. A. Sawadi, "Chapter new radiation pattern-reconfigurable 60-GHz antenna for 5G communications," 2019.